Quantitative prediction of human pregnane X receptor and cytochrome P450 3A4 mediated drug-drug interaction in a novel multiple humanized mouse line

Maki Hasegawa, Yury Kapelyukh, Harunobu Tahara, Jost Seibler, Anja Rode, Sylvia Krueger, Dongtao N. Lee, C. Roland Wolf, Nico Scheer

Kyowa Hakko Kirin Co., Ltd., 1188 Shimotogari, Nagaizumi-cho, Sunto-gun Shizuoka 411-8731, Japan (MH, HT).

CXR Biosciences Limited, James Lindsay Place, Dundee DD1 5JJ, United Kingdom (YK, DNL, CRW).

Cancer Research U.K. Molecular Pharmacology Unit, Biomedical Research Institute, Ninewells Hospital and Medical School, University of Dundee, Dundee DD1 9SY, United Kingdom (CRW).

TaconicArtemis, Neurather Ring 1, 51063 Köln, Germany (JS, AR, SK, NS)

Molecular Pharmacology Fast Forward. Published on May 31, 2011 as DOI: 10.1124/mol.111.071845
This article has not been copyedited and formatted. The final version may differ from this version.

Running title: PXR/CYP3A4-mediated drug-drug interaction in humanized mice

Address correspondence to:

Nico Scheer, PhD, TaconicArtemis, Neurather Ring 1, 51063 Koeln, Germany.

Tel.: +49 221 9645343; Fax: +49 221 9645321; Email: nico.scheer@taconicartemis.com

Number of text pages: 38

Number of Tables: 2

Number of Figures: 6

Number of references: 47

Number of words in Abstract: 199

Number of words in Introduction: 819

Number of words in Discussion: 2231

Nonstandard abbreviations used:

CAR, constitutive androstane receptor; CYP, cytochrome P450; DBF, dibenzylfluorescein; ES cells, embryonic stem cells; huCAR, humanized constitutive androstane receptor mice; huCYP3A4/3A7, humanized Cytochrome P450 3A4/3A7 mice; huPXR, humanized pregnane X receptor mice; MDZ, midazolam; PCN, pregnenolone-16∝-carbonitrile; PIO, pioglitazone; PXR, pregnane X receptor; RIF, rifampicin; RT-PCR, reverse transcription-polymerase chain reaction; SUL, sulfinpyrazone; TRZ, triazolam

Molecular Pharmacology Fast Forward. Published on May 31, 2011 as DOI: 10.1124/mol.111.071845
This article has not been copyedited and formatted. The final version may differ from this version.

Abstract

Cytochrome P450 (CYP) 3A4 is the predominant CYP enzyme expressed in human liver and intestine and it is involved in the metabolism of approximately 50% of clinically used drugs. Due to the differences in the multiplicity of *CYP3A* genes and the poor correlation of substrate specificity of CYP3A proteins between species, the extrapolation of CYP3A-mediated metabolism of a drug from animals to man is difficult. This situation is further complicated by the fact that the predictability of the clinically common drug-drug interaction of pregnane X receptor (PXR)-mediated CYP3A4 induction by animal studies is limited due to marked species differences in the interaction of many drugs with this receptor. Here we describe a novel multiple humanized mouse line that combines a humanization for PXR, the closely related constitutive androstane receptor (CAR) and a replacement of the mouse *Cyp3a* cluster with a large human genomic region carrying *CYP3A4* and *CYP3A7*. We provide evidence that this model shows a human-like CYP3A4 induction response to different PXR activators, that it allows the ranking of these activators according to their potency to induce CYP3A4 expression in the human liver and that it provides an experimental approach to quantitatively predict PXR/CYP3A4-mediated drug-drug interactions in humans.

Molecular Pharmacology Fast Forward. Published on May 31, 2011 as DOI: 10.1124/mol.111.071845
This article has not been copyedited and formatted. The final version may differ from this version.

Introduction

CYP enzymes play a major role in the oxidation of xenobiotics and endogenous compounds. In humans, 57 active P450 genes have been identified (Nelson et al., 2004), but only a limited number of those are involved in drug metabolism (Nebert and Russell, 2002). In this regard, the *CYP3A* subfamily is of particular importance. It contains four members, *CYP3A4*, *CYP3A5*, *CYP3A7* and *CYP3A43*. While the function of CYP3A43 is less well understood and CYP3A7 is a fetal form that is rarely expressed in adults, CYP3A5 and CYP3A4 both can contribute to the oxidative bio-transformation of drugs (Nebert and Russell, 2002; Williams et al., 2002). CYP3A4 is generally regarded as the cytochrome P450 of greatest importance in drug metabolism as it is the most abundant hepatic and intestinal CYP enzyme, the substrate specificity is extremely broad and it contributes to more than 50% of the primary metabolism of drugs currently on the market (de Wildt et al., 1999). CYP3A5 has an equal or reduced metabolic capability for CYP3A4 probe substrates (Williams et al., 2002), but it is polymorphic and is only expressed in 25% of Caucasians and approximately 50% of African Americans (Kuehl et al., 2001).

More than hundred putatively functional *Cyp* genes have been described in the mouse (Nelson et al., 2004). The presence of more functional *Cyp* genes in the mouse relative to humans is also reflected in the organization of the *Cyp3a* cluster, which in the mouse comprises eight functional genes. Seven of these, *3a57*, *3a16*, *3a41*, *3a44*, *3a11*, *3a25* and *3a59*, are located in close proximity to each other within approximately 0.8 Mb of mouse chromosome 5, while *3a13*, albeit on the same chromosome, is separated from the other genes by more than 7 Mb (Nelson et al., 2004). The comparison of the amino acid identity shows that a clear assignment of orthologous pairs between human and mouse CYP3A proteins is not possible (van Herwaarden et al., 2007). However, based on sequence similarity, abundance, tissue distribution and regulation of expression, mouse *Cyp3a11* is generally considered as most homologous to human *CYP3A4* (Anakk et al., 2004; Yanagimoto et al., 1997). *Cyp3a41* and

Molecular Pharmacology Fast Forward. Published on May 31, 2011 as DOI: 10.1124/mol.111.071845
This article has not been copyedited and formatted. The final version may differ from this version.

Cyp3a44 are female-specific isoforms with highest expression in the liver (Anakk et al., 2004; Sakuma et al., 2000). *Cyp3a16* is expressed in the fetal liver, which is lost after birth (Itoh et al., 1994). *Cyp3a25* and *Cyp3a13* are expressed predominantly in the liver, but the levels are much lower than those of *Cyp3a11* (Dai et al., 2001; Yanagimoto et al., 1997). Expression and function of *Cyp3a57* and *Cyp3a59* are poorly characterized.

As a consequence of the differences in multiplicity, expression level, tissue distribution, gender bias and substrate specificity of CYPs in different species, it is difficult to make predictions on the oxidative metabolism of a drug in humans based on the results obtained in animal studies. Furthermore, marked species differences in the regulation of CYP3A expression have been observed. Two of the key proteins involved in the regulation of CYP3A4 expression are the pregnane X receptor (PXR) and the constitutive androstane receptor (CAR), which both interact with a large variety of different drugs (reviewed in (Stanley et al., 2006)). The affinities of different ligands for these receptors vary significantly between species. For example, the macrocyclic antibiotic rifampicin (RIF) is more selective for the human receptor, while the synthetic C21 steroid pregnenolone-16∝-carbonitrile (PCN) is a potent ligand of mouse, but not human PXR (Xie et al., 2000). These differences in nuclear receptor interaction with various compounds clearly limit the utility of animal models in the prediction of clinically relevant drug-drug interactions by PXR or CAR-mediated induction of CYP3A4.

One way to overcome these limitations is the generation of humanized mouse models. Many such models have become available over the last few years (reviewed in (Cheung and Gonzalez, 2008)). For example, humanized mouse models for PXR (Ma et al., 2007; Scheer et al., 2010; Scheer et al., 2008; Xie et al., 2000), CAR (Scheer et al., 2008; Zhang et al., 2002) and CYP3A4 (Granvil et al., 2003; van Herwaarden et al., 2007; Yu et al., 2005) have been described by various groups. By combining two of these modifications a PXR/CYP3A4 double humanized model was successfully generated (Ma et al., 2008). In this model

Molecular Pharmacology Fast Forward. Published on May 31, 2011 as DOI: 10.1124/mol.111.071845
This article has not been copyedited and formatted. The final version may differ from this version.

CYP3A4 expression was inducible by the human specific PXR activator RIF, but not the mouse specific PXR agonist PCN. However, the mouse *Cyp3a* genes in this model were not deleted. As a consequence both mouse and human enzymes could potentially contribute to the metabolism of a compound, resulting in a mixed profile of drug metabolism. Furthermore, CAR was not humanized in this model, limiting its use in studying nuclear receptor/CYP3A4-mediated drug-drug interactions.

Here we describe the generation of a novel CYP3A4/3A7 humanized mouse line (huCYP3A4/3A7). In contrast to previous random transgenesis approaches we have used a sophisticated targeted insertion strategy to replace the seven closely linked mouse *Cyp3a* genes on chromosome 5 with a human BAC carrying *CYP3A4* and *CYP3A7*. The basal hepatic CYP3A4 expression was relatively low, but was highly inducible with the mouse specific PXR activator PCN, but not the human specific activator RIF. Expression in the intestine was constitutively high and was also inducible, though compared to the liver the magnitude of the intestinal induction response was lower. When crossed with the previously described humanized mouse models for PXR (huPXR) (Scheer et al., 2010) and CAR (huCAR) (Scheer et al., 2008), the induction response with the above inducers in the huPXR/huCAR/huCYP3A4/3A7 mouse line was reversed. We show that the huPXR/huCAR/huCYP3A4/3A7 model allows the ranking of different PXR activators according to their potency to induce CYP3A4 expression in humans and that this model might be a useful tool to quantitatively predict PXR/CYP3A4-mediated drug-drug interactions in the clinic.

Molecular Pharmacology Fast Forward. Published on May 31, 2011 as DOI: 10.1124/mol.111.071845
This article has not been copyedited and formatted. The final version may differ from this version.

Materials and Methods

Animal husbandry. Mice were kept as described previously (Scheer et al., 2008). If animals were shipped to a different location they were allowed to acclimatize for at least 5 days prior to an experimental procedure.

Vector construction and embryonic stem (ES) cell targeting to generate Cyp3a$^{-/-}$/Cyp3a13$^{+/+}$ and huCYP3A4/3A7 mice. In all cases, culture and targeted mutagenesis of ES cells were carried out as previously described (Hogan et al., 1994). C57BL/6 mouse ES cells were used for all experiments. The technical details of the vector construction and ES cell work that was performed in order to generate Cyp3a$^{-/-}$/Cyp3a13$^{+/+}$ and huCYP3A4/3A7 mice is described in the Supplementary Materials and Methods.

Generation and molecular characterization of Cyp3a$^{-/-}$/3a13$^{+/+}$ and huCYP3A4/3A7 mice. Chimeric Cyp3a$^{-/-}$/3a13$^{+/+}$ and huCYP3A4/3A7 mice were generated by injection of correctly targeted ES cell clones into BALBc-blastocysts, which were transferred into foster mothers as previously described (Hogan et al., 1994). Litters from these fosters were visually inspected and chimerism was determined by hair colour. Highly chimeric animals were used for further breeding in a C57BL/6 genetic background. While Cyp3a$^{-/-}$/3a13$^{+/+}$ chimeras were crossed to WT animals, an efficient Flp-deleter (Flpe-deleter) strain was used in the case of huCYP3A4/3A7 mice in order to remove the selection markers. Flpe mice express the corresponding recombinase in the germ line and they have been generated in house on a C57BL/6 genetic background. Germ line transmission was obtained for both genotypes and a successful in vivo deletion of selection markers could be confirmed for the huCYP3A4/3A7 mice. Heterozygous offspring emerging from the two mouse lines were further crossed to generate homozygous Cyp3a$^{-/-}$/3a13$^{+/+}$ and huCYP3A4/3A7 mice, respectively. The genotype of these mouse lines was determined by combination of the PCRs listed in Supplementary Table 1.

Molecular Pharmacology Fast Forward. Published on May 31, 2011 as DOI: 10.1124/mol.111.071845
This article has not been copyedited and formatted. The final version may differ from this version.

Animals and Treatments. All animal studies were conducted in accordance with the guiding principles for the care and use of laboratory animals and procedures were either carried out under a United Kingdom Home Office license with approval by the Ethical Review Committee, University of Dundee, or approved by the Committee for Animal Experiments in Kyowa Hakko Kirin Co., Ltd. Homozygous 8-12 weeks old male Cyp3a$^{-/-}$/3a13$^{+/+}$, huCYP3A4/3A7 and huPXR/huCAR/huCYP3A4/3A7 mice were used for all experiments. WT C57BL/6 animals of the same genetic background and age purchased from Harlan UK Limited (Bicester, Oxon, UK) were used for control experiments when applicable. Mice were dosed by oral administration or i.p. injection with either corn oil, pregnenolone-16∝-carbonitrile (PCN) (Sigma-Aldrich, St. Louis, MO), rifampicin (RIF) (Sigma-Aldrich), sulvinpyrazone (SUL) (Prestwick Chemical, Illkirch, France), pioglitazone (PIO) (LKT Labs, St Paul, MN) or triazolam (TRZ) (Sigma-Aldrich) according to the specification in the results section and were sacrificed 24 h post last dose.

Blood sampling. Blood samples (about 15 μl) were collected from the tail vein at the time points specified in the results section. The blood samples were centrifuged and the plasma samples were collected. The plasma samples were stored at −20°C until analysis.

Quantification of rifampicin, sulfinpyrazone, pioglitazone and triazolam in plasma. Plasma samples were analyzed by a liquid chromatography tandem mass spectrometry (LC/MS/MS) using an API Sciex 4000 (Applied Biosystems, Foster City, CA). The technical details of the analysis of the plasma samples are described in the Supplementary Materials and Methods.

Pharmacokinetic analysis. The pharmacokinetic parameters for RIF, SUL, PIO and TRZ were obtained by non-compartmental analysis. Log-transformed plasma concentrations were plotted against time. The slope of the elimination phase (λ_z) was estimated by linear regression. Maximum plasma concentration (C_{max}) and time to C_{max} (t_{max}) were obtained directly from the observed values. Apparent $t_{1/2}$ was obtained as $\ln 2/\lambda_z$. Area under the plasma

Molecular Pharmacology Fast Forward. Published on May 31, 2011 as DOI: 10.1124/mol.111.071845
This article has not been copyedited and formatted. The final version may differ from this version.

concentration-time curve (AUC) from time 0 to the last data point (AUC_{0-t}) was calculated using the linear trapezoidal method. AUC after the last data point ($AUC_{\lambda z}$) was estimated by extrapolating with λ_z. The sum of AUC_{0-t} and $AUC_{\lambda z}$ was regarded as $AUC_{0-\infty}$.

Quantitative Reverse Transcriptase PCR (qRT-PCR). Human *CYP3A4* and *CYP3A7* and murine *Cyp3a13* and *Cyp2c55* RNA was analyzed by quantitative RT-PCR. Liver and intestine samples were preserved in RNAlater solution (QIAGEN, Hilden, Germany) and incubated at 4°C overnight, then stored at -20°C until RNA isolation. The organ samples were homogenized and total RNA was extracted using the QIAGEN RNeasy Plus Mini. The technical details of the analysis of the qRT-PCR are described in the Supplementary Materials and Methods.

Microsomal Preparation. Mouse liver and intestinal microsomes were prepared as described recently (Scheer et al., 2008).

Immunoblot Analysis. For Western Blot analysis, 3 µg liver microsomal protein and duodenum microsomal protein from pooled mouse samples was separated by SDS-PAGE, electropheretically transferred to nitrocellulose membranes, and probed using a polyclonal rabbit anti-CYP3A4 (BD Gentest, catalogue #458234, Franklin Lakes, NJ). The secondary antibody was anti-rabbit HRP conjugate (GE Healthcare, Little Chalfont, Buckinghamshire, UK). Detection of immunoreactive proteins was performed by an enhanced chemiluminescence blot detection system (GE Healthcare). 0.1 pmol of human CYP3A4 baculosomes (Invitrogen, catalogue #P2377, Carlsbad, CA) were used as a CYP3A4 standard.

Measurement of TRZ, midazolam, dibenzylfluorescein and testosterone oxidation in microsomes. The technical details of measuring the oxidation of TRZ, midazolam (MDZ) and dibenzylfluorescein (DBF) (BD Gentest) are described in the Supplementary Materials and Methods.

Molecular Pharmacology Fast Forward. Published on May 31, 2011 as DOI: 10.1124/mol.111.071845
This article has not been copyedited and formatted. The final version may differ from this version.

Statistics. Statistical significance was assessed to determine differences between mouse groups using a two-tailed, paired, Student's t test or a one-way analysis of variance (ANOVA) with Dunnett test as indicated. The criterion for statistical significance was $P < 0.05$.

Molecular Pharmacology Fast Forward. Published on May 31, 2011 as DOI: 10.1124/mol.111.071845
This article has not been copyedited and formatted. The final version may differ from this version.

Results

Generation of Cyp3a$^{-/-}$/3a13$^{+/+}$, huCYP3A4/3A7 and huPXR/huCAR/huCYP3A4/3A7 mice. Mice with a deletion of the seven closely linked mouse *Cyp3a* genes on chromosome 5 has been previously reported (Scheer et al., 2010). To summarize, these Cyp3a$^{-/-}$/3a13$^{+/+}$ mice were created from a C57BL/6 mouse embryonic stem (ES) cell line that was double targeted with *loxP* sites at the *Cyp3a57* and *Cyp3a59* loci .The mouse *Cyp3a* cluster with the exception of *Cyp3a13*, which is located 7Mb away, was then deleted by subsequent Cre-mediated recombination between the *loxP* sites (Fig. 1A-E). Using this procedure all exons and introns from *Cyp3a57*, *Cyp3a16*, *Cyp3a41*, *Cyp3a44*, *Cyp3a11* and *Cyp3a25* were deleted including exons 1 to 4 and the promoter of *Cyp3a59*.

huCYP3A4/3A7 mice were generated from the *Cyp3a* deleted ES cells described above by Cre-mediated insertion of a modified human BAC containing *CYP3A4* and *CYP3A7* via the non-interacting (heterospecific) Cre recombination sites *loxP* and *lox5171* (Lee and Saito, 1998) (Fig. 1F-H). This approach is similar, though not identical, to the recombinase-mediated genomic replacement of the mouse α globin regulatory domain with the human synthetic region described by Smith and co-workers (Wallace et al., 2007). In contrast to their approach, we flanked the mouse *Cyp3a* cluster with a pair of homospecific *loxP* sites in addition to the heterospecific *lox*-sites required for insertion of the human BAC, which in an intermediate step allowed us to delete the mouse *Cyp3a* locus as described above. Compared to the α globin humanization this intermediate deletion step necessitated an additional round of ES cell transfection, but had the advantage of also generating the Cyp3a$^{-/-}$/3a13$^{+/+}$ mice. Furthermore, our approach used a different selection marker system to achieve high stringency for the selection of humanized clones with a correct Cre-mediated insertion via the heterospecific *lox* sites. High stringency is important due to the low efficiency of site specific insertion of large genomic sequences by recombinases in ES cells (Wallace et al., 2007). While a hypoxanthine-phosphoribosyl-transferase complementation system was used

Molecular Pharmacology Fast Forward. Published on May 31, 2011 as DOI: 10.1124/mol.111.071845
This article has not been copyedited and formatted. The final version may differ from this version.

previously, we employed an ATG-deficient Neomycin cassette which was complemented by a promoter and an ATG introduced into the *Cyp3a* knockout locus. The former requires the use of an hypoxanthine-phosphoribosyl-transferase-deficient ES cell line, whereas Neomycin confers resistance to G418, to which all eukaryotic cells are sensitive. Therefore, the Neomycin complementation approach allowed us to use a standard C57BL/6 ES cell line and in principle is transferable to any eukaryotic cell line. The BAC that was used to generate the huCYP3A4/3A7 mice contains approximately 125 kb of genomic human DNA comprising the *CYP3A4* and *CYP3A7* gene and including a 37 kb sequence upstream of the *CYP3A4* transcriptional start site. The integrity of the inserted BAC was confirmed in targeted ES cells by Southern blot and PCR analysis and the coding region of the *CYP3A4* gene was additionally sequenced to ensure that it is in accordance with the reference sequence listed by the Human Cytochrome P450 Allele Nomenclature Committee (http://www.cypalleles.ki.se/cyp3a4.htm).

huPXR/huCAR/huCYP3A4/3A7 mice were obtained by breeding of huCYP3A4/3A7 mice with the previously described huCAR and huPXR mice (Scheer et al., 2010; Scheer et al., 2008). Homozygous $Cyp3a^{-/-}/3a13^{+/+}$, huCYP3A4/3A7 and huPXR/huCAR/huCYP3A4/3A7 mice appeared normal, could not be distinguished from WT mice and had normal survival rates and fertility (data not shown).

Analysis of the basal and inducible CYP3A4 and CYP3A7 expression in huCYP3A4/3A7 and huPXR/huCAR/huCYP3A4/3A7 mice. Hepatic and intestinal *CYP3A4* mRNA levels were quantified by reverse transcriptase (qRT)-PCR (TaqMan®) in adult mice treated with either vehicle, RIF (10 mg/kg i.p. daily for three days) or PCN (10 mg/kg i.p. daily for two days). The average ΔCt values of 7.8 and 7.4 in the huCYP3A4/3A7 and huPXR/huCAR/huCYP3A4/3A7 mice suggested that the constitutive level of hepatic *CYP3A4* mRNA in both models was relatively low (Supplementary Table 2). In comparison, the average ΔCt value for hepatic *Cyp3a11* expression in untreated WT animals was -0.7

Molecular Pharmacology Fast Forward. Published on May 31, 2011 as DOI: 10.1124/mol.111.071845
This article has not been copyedited and formatted. The final version may differ from this version.

(data not shown) suggesting a much higher level of expression than *CYP3A4* (a low ΔCt value reflecting a high expression level). Basal *CYP3A4* ΔCt values in the duodenum of the huCYP3A4/3A7 and huPXR/huCAR/huCYP3A4/3A7 mice were 6.6 and 5.9, respectively (Supplementary Table 2), compared to 6.2 for *Cyp3a11*. Therefore, the constitutive intestinal expression level of *CYP3A4* in the transgenic mice appears comparable to *Cyp3a11* in WT animals. As expected, no *CYP3A4* mRNA was detected in the liver or intestine of Cyp3a$^{-/-}$/3a13$^{+/+}$ or WT animals (data not shown).

A significant ~31-fold induction of *CYP3A4* mRNA levels was observed in the liver of the huCYP3A4/3A7 animals treated with PCN, but not in huPXR/huCAR/huCYP3A4/3A7 mice (Fig. 2A). In contrast, RIF induced hepatic *CYP3A4* mRNA in the multiple humanized mice by approximately 200-fold, but had no effect in the huCYP3A4/3A7 mouse line. Though the same trend in the induction profile was observed in the duodenum, this effect was less marked and was not statistically significant (Fig. 2B).

CYP3A7 mRNA could not be detected in the liver or intestine of the untreated adult huCYP3A4/3A7 or huPXR/huCAR/huCYP3A4/3A7 male mice. Interestingly, hepatic *CYP3A7* mRNA levels were detectable in huCYP3A4/3A7 mice treated with PCN and in RIF-treated huPXR/huCAR/huCYP3A4/3A7 animals but not vice versa (Supplementary Table 2). However, with average ΔCt values of 13.1 in the liver of the PCN treated huCYP3A4/3A7 mice and 10.4 in the RIF induced huPXR/huCAR/huCYP3A4/3A7 model, the expression was almost 2000-fold lower than the induced *CYP3A4* expression in the liver of each of the corresponding mouse lines suggesting that the induced hepatic *CYP3A7* mRNA expression in these models is very low.

We then determined CYP3A4 protein expression by Western blot analysis with a human CYP3A4 specific antibody. These data confirmed the mRNA analysis in that the hepatic CYP3A4 protein level in the vehicle treated huCYP3A4/3A7 and huPXR/huCAR/huCYP3A4/3A7 mice was low and was strongly inducible with PCN and RIF

Molecular Pharmacology Fast Forward. Published on May 31, 2011 as DOI: 10.1124/mol.111.071845
This article has not been copyedited and formatted. The final version may differ from this version.

in the huCYP3A4/3A7 and huPXR/huCAR/huCYP3A4/3A7, respectively (Fig. 2C). In order to compare the basal hepatic CYP3A4 protein levels in the transgenic mice with that in human liver, we also included pooled human liver microsomes (pHLM) from different donors, as well as liver microsomes from single human donors with low (SD118) and high (SD002) CYP3A4 expression in the Western blot analysis. The results show that the basal hepatic CYP3A4 expression in the transgenic mice is higher than that in the human donor with low expression, in which expression was below the limit of detection by Western blot, but significantly lower than that in pooled human liver microsomes or in the donor with high expression. In the duodenum, the basal CYP3A4 expression level was higher in both models and it was only marginally inducible with PCN and RIF in the huCYP3A4/3A7 huPXR/huCAR/huCYP3A4/3A7 mice, respectively (Fig. 2D). In this organ RIF seems to decrease the CYP3A4 expression level in the huCYP3A4/3A7 model for unknown reasons. No CYP3A4 protein was detected in the liver or intestine of Cyp3a$^{-/-}$/3a13$^{+/+}$ or WT animals (data not shown).

We have also investigated the induction of *Cyp3a13* and *Cyp2c55* mRNA expression in Cyp3a$^{-/-}$/3a13$^{+/+}$, huCYP3A4/3A7 and huPXR/huCAR/huCYP3A4/3A7 mice, which is described in the Supplementary Text 1, Supplementary Table 2 and Supplementary Figure 1. In summary, *Cyp2c55* but not *Cyp3a13* mRNA expression was inducible with PCN or RIF in the corresponding treatment groups.

The CYP3A4 protein expressed in huCYP3A4/3A7 and huPXR/huCAR/huCYP3A4/3A7 mice is catalytically active. To further investigate the catalytic activity of the expressed CYP3A4 protein we measured the metabolism of the CYP3A4 probe substrates triazolam (TRZ), dibenzylfluorescein (DBF), midazolam (MDZ) and testosterone in microsomes from PCN- and RIF-treated animals. In order to assess the contribution of CYP3A4 in the metabolism of these compounds, we also included microsomes from the Cyp3a$^{-/-}$/3a13$^{+/+}$ animals. TRZ, DBF and MDZ oxidation determined by the formation of the metabolites α-

Molecular Pharmacology Fast Forward. Published on May 31, 2011 as DOI: 10.1124/mol.111.071845
This article has not been copyedited and formatted. The final version may differ from this version.

hydroxytriazolam, fluorescein and 4-hydroxymidazolam was significantly induced in the liver microsomes from huCYP3A4/3A7 mice treated with PCN by ~4, 3 and 3-fold, respectively, but neither in the PCN treated huPXR/huCAR/huCYP3A4/3A7 nor Cyp3a$^{-/-}$/3a13$^{+/+}$ animals (Fig. 3A). In contrast, RIF induced the oxidation of these compounds by ~24, 18 and 15-fold in the liver microsomes from huPXR/huCAR/huCYP3A4/3A7 mouse line only. The formation of the 1-hydroxymidazolam metabolite from MDZ and the 6ß-hydroxytestosterone metabolite from testosterone was also specifically increased by ~4 and 5-fold, respectively, in the liver microsomes from PCN treated huCYP3A4/3A7 mice and by ~11 and 29-fold in the RIF treated huPXR/huCAR/huCYP3A4/3A7 animals (data not shown).

Similar effects were observed in the intestinal microsomes. While the magnitude of induction following PCN treatment was comparable between the liver and duodenum, the effect of RIF in the intestine appeared to be slightly lower than in the liver (Fig. 3B). Namely, PCN induced α-hydroxytriazolam, fluorescein, 4-hydroxymidazolam and 1-hydroxymidazolam formation by ~4, 3, 3 and 3-fold in the duodenum of the huCYP3A4/3A7 mice and RIF by ~10, 8, 9 and 10-fold in the huPXR/huCAR/huCYP3A4/3A7 model, respectively. 6β-Hydroxytestosterone generated by duodenum microsomes was at or below the lower limit of quantification, which did not allow comparison of the activities between the experimental groups (data not shown).

In summary, these data are in general agreement with the CYP3A4 expression levels detected by qRT-PCR and Western blot analysis and they verify that the expressed CYP3A4 protein in the humanized mouse lines is active. Interestingly, the intestinal induction of *CYP3A4* mRNA by rifampicin was weak at about 2.5-fold, while the same treatment increased the catalytic activity in the microsomes from this tissue by 8 to 10-fold for TRZ, DBF and MDZ. The reason for this difference is currently not known, but cannot be due to the induction of other genes that might metabolise the CYP3A4 probe substrates, because no induction was observed in samples from the Cyp3a$^{-/-}$/3a13$^{+/+}$ mice. The increase in catalytic activity therefore appears to be CYP3A4-dependent.

Molecular Pharmacology Fast Forward. Published on May 31, 2011 as DOI: 10.1124/mol.111.071845
This article has not been copyedited and formatted. The final version may differ from this version.

Effects of rifampicin, sulfinpyrazone and pioglitazone on CYP3A4 expression and pharmacokinetics of triazolam in huCYP3A4/3A7 and huPXR/huCAR/huCYP3A4/3A7 mice. In order to assess the utility of the huPXR/huCAR/huCYP3A4/3A7 mice to rank different PXR activators according to their potency to induce CYP3A4 expression and to quantitatively predict PXR/CYP3A4-mediated drug-drug interactions in humans, the following study was carried out. huCYP3A4/3A7 (control) and huPXR/huCAR/huCYP3A4/3A7 mice were given oral daily doses of vehicle or the strong, moderate and weak human PXR activators RIF, sulfinpyrazone (SUL) and pioglitazone (PIO) for 4 days (Ripp et al., 2006; Sinz et al., 2006). Serial blood samples were taken on day 1 and day 4 to determine the pharmacokinetics of the compounds and to establish the doses required to obtain similar exposures to those measured in humans under standard clinical conditions. Five mg/kg TRZ was orally administered to all animals on day 5, followed by serial blood sampling to investigate the effect of the different PXR activators on the pharmacokinetics of this CYP3A4 probe substrate. Subsequently, the liver and intestine were prepared to measure the impact of the PXR activators on CYP3A4 expression in these organs.

The plasma concentration-time curves and pharmacokinetic parameters for RIF (tested doses 1, 3 and 10 mg/kg), SUL (0.5, 2 and 10 mg/kg) and PIO (2, 10 and 50 mg/kg) in the huPXR/huCAR/huCYP3A4/3A7 mice are shown in Fig. 4A-C and Table 1, respectively. For patients receiving standard clinical doses of RIF (600 mg), SUL (200 mg) and PIO (45 mg) the reported pharmacokinetic parameters were 8500 ng/ml (C_{max}) and 28100 ng·h/ml ($AUC_{0-\infty}$) for RIF (Polk et al., 2001), 19500 ng/ml (C_{max}) and 79600 ng·h/ml ($AUC_{0-\infty}$) for SUL (Bradbrook et al., 1982) and 1300-1600 ng/ml (C_{max}) and 14600-17400 ng·h/ml ($AUC_{0-\infty}$) for PIO (Budde et al., 2003). Based on these data we estimated that doses of 3-10 mg/kg RIF, 2-10 mg/kg SUL and 2 mg/kg PIO resulted in a similar exposure in mice as in humans receiving a standard dose of these drugs. Furthermore, the plasma unbound fraction of RIF (0.18), SUL (0.0123) and PIO (0.015) in the huPXR/huCAR/huCYP3A4/3A7 mice was similar to that in

Molecular Pharmacology Fast Forward. Published on May 31, 2011 as DOI: 10.1124/mol.111.071845
This article has not been copyedited and formatted. The final version may differ from this version.

humans (0.25 for RIF, 0.0169 for SUL and <0.03 for PIO) (Fahmi et al., 2009; Schlicht et al., 1985; Tornio et al., 2008). The plasma concentration-time curves and pharmacokinetic parameters for the three compounds in the huCYP3A4/3A7 mice were very similar to the huPXR/huCAR/huCYP3A4/3A7 animals (data not shown).

We then measured the effect of the different PXR activators on the *CYP3A4* mRNA levels in the liver and intestine of the two transgenic mouse lines. Compared to the vehicle treated control mice RIF doses of 3 and 10 mg/kg significantly increased the hepatic *CYP3A4* mRNA level in the huPXR/huCAR/huCYP3A4/3A7 mouse line by 15 and 44-fold, respectively (Fig. 5A). The stronger induction of *CYP3A4* mRNA expression in the liver by i.p. administration of 10 mg/kg RIF (~200-fold, see above), is probably due to a higher hepatic exposure to the PXR activator following injection. Two and 10 mg/kg SUL increased the *CYP3A4* mRNA levels in the liver of this mouse line by 4.2 and 10.3-fold, respectively, but only the changes at the higher dose were statistically significant. No induction of hepatic *CYP3A4* expression was seen in the huCYP3A4/3A7 model treated with RIF or SUL, confirming that both compounds predominantly interact with the human, but not the mouse PXR receptor. No significant change was observed at the relevant PIO dose of 2 mg/kg (Fig. 5A). However, the higher PIO doses of 10 and 50 mg/kg increased the hepatic *CYP3A4* mRNA levels by 3.0 and 4.7-fold, with statistical significance at the 50 mg/kg dose. Accordingly, the potency of RIF, SUL and PIO to induce *CYP3A4* expression in the liver of the huPXR/huCAR/huCYP3A4/3A7 mouse line reflects their categorization as strong, moderate and weak activators of human PXR, respectively (Ripp et al., 2006; Sinz et al., 2006). The induction of intestinal *CYP3A4* mRNA expression by the different compounds was less pronounced and changes were generally statistically insignificant. A slight (0.6-fold) decrease of *CYP3A4* mRNA was observed in the intestine of the huPXR/huCAR/huCYP3A4/3A7 treated with 50 mg/kg PIO, but the significance of this observation would need to be verified with additional studies (Fig. 5B).

Molecular Pharmacology Fast Forward. Published on May 31, 2011 as DOI: 10.1124/mol.111.071845
This article has not been copyedited and formatted. The final version may differ from this version.

The plasma concentration-time curves for TRZ in the huPXR/huCAR/huCYP3A4/3A7 mouse line following administration of RIF, SUL and PIO are shown in Fig. 6 and the pharmacokinetic parameters are summarized in Table 2. Both RIF and SUL treatment resulted in an AUC decrease of TRZ in a dose dependent manner. At the clinically relevant dose range of 3–10 mg/kg of RIF the TRZ AUC was significantly decreased by 63-91%. For SUL the observed decrease in the 2-10 mg/kg dose range was 15-37%, with statistical significance at the 10 mg/kg dose. No dose dependent effects on the TRZ AUC were observed in the huCYP3A4/3A7 model and all changes were not statistically significant (data not shown). For PIO, the decrease in the TRZ AUC in the huPXR/huCAR/huCYP3A4/3A7 model at the clinically relevant 2 mg/kg dose was 2%, while the 50 mg/kg dose appeared to increase the TRZ exposure. However, none of the changes observed with PIO were statistically significant.

In the RIF treated animals we also analysed the changes in the pharmacokinetics of the 1-OH and α-OH TRZ metabolites. In the huPXR/huCAR/huCYP3A4/3A7 mice, but not in the huCYP3A4/3A7 animals, the AUC of both metabolites was significantly decreased, e.g. by 65% and 68%, respectively, in the 10 mg/kg treatment group (data not shown), despite the induction of CYP3A4 in this model. This is in agreement with a similar decrease in the plasma exposure of midazolam metabolites in RIF treated cynomolgus monkeys and is probably a result of the additional induction of phase II enzymes and drug transporters by PXR (Kim et al., 2010).

Molecular Pharmacology Fast Forward. Published on May 31, 2011 as DOI: 10.1124/mol.111.071845
This article has not been copyedited and formatted. The final version may differ from this version.

Discussion

In this paper we describe the generation and characterization of a novel CYP3A4 humanized mouse line that carries a replacement of the seven chromosomally closely linked murine *Cyp3a* genes with a large human genomic region carrying *CYP3A4* and *CYP3A7*. A similar approach to replace large sequences of mouse genomic DNA with a syntenic region of human DNA was recently described for the α globin regulatory domain (Wallace et al., 2007). The use of a modified strategy allowed us to generate knockout control mice, Cyp3a$^{-/-}$/3a13$^{+/+}$, carrying a deletion of the major part of the mouse *Cyp3a* cluster. Furthermore, as a consequence of using a different selection marker, our approach can be applied to any eukaryotic cell type and can therefore be used widely for the exchange of genomic regions between species.

The targeted insertion strategy applied in the present work distinguishes our huCYP3A4/3A7 model from other existing CYP3A4 humanized mouse lines. Compared to the recently described random transgenic mouse line generated with the same BAC that we have used in our model (Granvil et al., 2003), the huCYP3A4/3A7 model has the advantage that it combines a knockout of the major part of the mouse *Cyp3a* cluster with the humanization of CYP3A4. This minimizes a potential contribution of mouse Cyp3a proteins to the metabolism of a CYP3A4 probe substrate in these mice. However, it should be noted that despite the absence of seven functional mouse *Cyp3a* genes in the huCYP3A4/3A7 mouse line, murine *Cyp3a13* was not deleted. The relatively low expression in the liver and intestine suggests that the relevance of Cyp3a13 in drug metabolism is limited. This assumption is supported by the fact that compared to WT animals, the catalytic activity of liver and intestinal microsomes from the Cyp3a$^{-/-}$/3a13$^{+/+}$ mouse line for a number of different Cyp3a probe substrates was markedly reduced, indicating that the major Cyp3a activity in the knockout animals was lost (data not shown). Furthermore, in contrast to Cyp3a11, hepatic and intestinal Cyp3a13 expression was not induced in response to PXR activation. Therefore, Cyp3a13-mediated

Molecular Pharmacology Fast Forward. Published on May 31, 2011 as DOI: 10.1124/mol.111.071845
This article has not been copyedited and formatted. The final version may differ from this version.

changes in the metabolism of a CYP3A4 probe substrate as a result of PXR activation should not occur.

An important implication of our cluster replacement strategy is that it significantly simplifies the combination of the *CYP3A4* humanized locus with additional transgenic modifications in a multiple humanized mouse line. While the conventional approach of crossing a random insertion of a human transgene with a knockout of the corresponding mouse gene(s) requires the combination of two independently segregating genetic loci, the *Cyp3a* knockout and *CYP3A4* humanization are linked in the huCYP3A4/3A7 model. Due to the fact that the recently published PXR and CAR humanized models were generated by a targeted insertion strategy as well (Scheer et al., 2010; Scheer et al., 2008), the combination of these different modifications in the multiple humanized huPXR/huCAR/huCYP3A4/3A7 model described in the present work was straightforward.

The expression of CYP3A4 under control of its own human promoter also distinguishes the huCYP3A4/3A7 model from the recently described mouse lines in which CYP3A4 is specifically expressed in the liver or intestine by using the apoE or villin promoter, respectively (van Herwaarden et al., 2007). Although a comparison has not been made, the basal hepatic CYP3A4 expression in the apoE-CYP3A4 mouse line appears to be significantly higher than in our huCYP3A4/3A7 model. The apoE-CYP3A4 model is well suited for studies requiring a high basal expression of CYP3A4 expression in the liver. However, the fact that because CYP3A4 expression in this model is not regulated by CAR or PXR, as it usually is in humans (Moore et al., 2000), precludes its use for the type of drug-drug interaction studies described here and which have an important clinical implication. In contrast to transgenic lines using heterologous promoters, this interaction can be reflected by models which contain the human *CYP3A4* regulatory sequences and therefore they can be important tools to study the drug-drug interactions caused by PXR-mediated induction of CYP3A4 expression in vivo. The extrapolation of the results from such studies to the human

Molecular Pharmacology Fast Forward. Published on May 31, 2011 as DOI: 10.1124/mol.111.071845
This article has not been copyedited and formatted. The final version may differ from this version.

situation is further complicated by the species-differences in PXR-interactions that have been observed for many drugs (Stanley et al., 2006). The huPXR/huCAR/huCYP3A4/3A7 model described in the present paper might offer a solution to such challenges and it overcomes some of the limitations of previously described mouse lines in that it combines the humanizations for both PXR and CAR with CYP3A4 and is deleted for the major part of the mouse *Cyp3a* cluster.

The finding of relatively low hepatic and robust intestinal CYP3A4 expression in adult huCYP3A4/3A7 males is in agreement with the observations in other models using the human *CYP3A4* promoter (Granvil et al., 2003; Yu et al., 2005). The reason for the low hepatic CYP3A4 expression in transgenic mice using the human promoter is currently unknown. However, it should be noted that in humans the basal hepatic CYP3A4 expression is highly variable, with very low levels in some individuals (Forrester et al., 1990) and we could show that the basal hepatic CYP3A4 expression in the transgenic mice lies in the range of levels that are observed in humans. Therefore, it can be speculated that the maintenance of transgenic mice in a protected environment with controlled nutrition might simply reflect the absence of exogenous PXR/CAR inducing agents in humans leading to low constitutive hepatic CYP3A4 levels. Other possible explanations might be the lack of interaction of certain mouse transcription factors with the human promoter or the deficiency of distant enhancer elements in the sequence that was used. CYP3A4 expression was found to be both age and sex dependent in the recently described random transgenic CYP3A4 humanized mouse line (Yu et al., 2005). In this model CYP3A4 was expressed in the liver of 2 and 4 weeks old transgenic females and males and was lost in 6 weeks old males, but continued to be constitutively expressed in adult females. Interestingly, we could not observe such a dimorphic regulation of CYP3A4 expression in the huCYP3A4/3A7 model. In our studies, it appears that hepatic CYP3A4 expression is low in both males and females throughout development and higher in the intestine (data not shown). These potential variations between

Molecular Pharmacology Fast Forward. Published on May 31, 2011 as DOI: 10.1124/mol.111.071845
This article has not been copyedited and formatted. The final version may differ from this version.

the models might be due to position effects as a consequence of different sites of integration in the mouse genome, differences in the length or integrity of the inserted human DNA sequence, genetic background or differences in diet. However, it should be noted that we have not systematically analyse the changes of CYP3A4 expression over time and this requires further studies.

The major aim of the present work was to evaluate whether the huPXR/huCAR/huCYP3A4 model would allow the ranking of different PXR activators according to their potency to induce CYP3A4 expression and the quantitative prediction of PXR/CYP3A4-mediated drug-drug interactions in humans. A first important finding in this regard was the induction of hepatic CYP3A4 mRNA, protein and catalytic activity by the human specific PXR activator rifampicin, while no induction response was seen with the more potent mouse PXR agonist PCN.

We then determined the doses of the strong, moderate and weak human PXR activators rifampicin, sulfinpyrazone and pioglitazone, which result in comparable exposures of these compounds in the transgenic mice as seen in humans under standard clinical conditions. At the relevant doses of 3-10 mg/kg and 2-10 mg/kg RIF and SUL led to a 15-44-fold and 4-10-fold induction of hepatic *CYP3A4* mRNA expression in the huPXR/huCAR/huCYP3A4/3A7 model, respectively, while no induction was observed in huCYP3A4/3A7 mice. At the clinically relevant dose of 2 mg/kg PIO did not induce *CYP3A4* mRNA expression in the liver of these mice. However, this expression was induced by 3.0 and 4.7-fold at the doses of 10 mg/kg and 50 mg/kg, respectively, which considerably exceed the normal clinical dose. For the three compounds tested, the results in the huPXR/huCAR/huCYP3A4/3A7 mice therefore predicted the ranking of different PXR activators according to their potency to induce CYP3A4 expression in man (Ripp et al., 2006; Sinz et al., 2006).

In order to assess whether the huPXR/huCAR/huCYP3A4/3A7 mouse line also permits quantitative predictions of human PXR/CYP3A4-mediated drug-drug interactions, we

Molecular Pharmacology Fast Forward. Published on May 31, 2011 as DOI: 10.1124/mol.111.071845
This article has not been copyedited and formatted. The final version may differ from this version.

measured the effects of the clinically relevant RIF, SUL and PIO doses on the pharmacokinetics of the CYP3A4 probe substrate triazolam in these mice and compared these to the described changes observed in human subjects. At the relevant doses RIF decreased the TRZ AUC by 63-91% and SUL by 15-37% in huPXR/huCAR/huCYP3A4/3A7 mice, while the effect of PIO was minimal and statistically insignificant. The decreases in the exposure of co-administered CYP3A4 probe substrates observed in the clinic were 73-96% for RIF (Backman et al., 1996; Chung et al., 2006; Hebert et al., 1992; Kyrklund et al., 2000; Villikka et al., 1997), 39% for SUL (Caforio et al., 2000) and 0-26% for PIO ((Prueksaritanont et al., 2001) and http://www.accessdata.fda.gov/drugsatfda_docs/label/2007/021073s031lbl.pdf). Therefore, the observed effects of the different PXR activators on the pharmacokinetics of a CYP3A4 substrate in the humanized mouse line are very similar to those reported in the clinic and the huPXR/huCAR/huCYP3A4/3A7 mouse model thus might allow quantitative predictions of such changes in humans. Compared to a recently published study evaluating the utility of a PXR humanized mouse line for quantitative predictions of PXR-mediated drug-drug interactions (Kim et al., 2008), the model described in the present work has the advantage of combining the humanization of both the 'mediator' (PXR) as well as the 'target' (CYP3A4) in this process. The same group also suggested the cynomolgus monkey as an alternative system for predicting PXR-mediated induction of CYP3A4 in humans (Kim et al., 2010). The huPXR/huCAR/huCYP3A4/3A7 model might negate the use of non-human primates for such studies. When comparing the results from our study with clinical observations, it should be noted, however, that published human data are based on the effect of the different PXR activators on the pharmacokinetic changes of a variety of CYP3A4 probe substrates, such as cyclosporine A, simvastatin, midazolam and triazolam. Therefore, a direct comparison of our results with human clinical data has to be drawn cautiously.

An interesting observation from the present study was that pioglitazone at a dose higher than the normal clinical dose (50 mg/kg) though inducing hepatic *CYP3A4* mRNA levels by 4.7-

Molecular Pharmacology Fast Forward. Published on May 31, 2011 as DOI: 10.1124/mol.111.071845
This article has not been copyedited and formatted. The final version may differ from this version.

fold did not decrease triazolam exposure in the huPXR/huCAR/huCYP3A4/3A7 mice. A potential explanation is that PIO is not only a CYP3A4 inducer via PXR, but also a mechanism based inhibitor of CYP3A4 (Sahi et al., 2003). As the induction of hepatic *CYP3A4* mRNA levels at this high dose is relatively weak, it is possible that the inhibitory effect of this compound predominates at these exposure levels. Therefore, another benefit of the transgenic mouse model might be its use in assessing the relative contribution of CYP3A4 induction and inhibition to the metabolism of a compound in vivo. However, further work will be required in order to verify this finding.

Compared to the liver, the induction of *CYP3A4* mRNA in the duodenum was less pronounced and these changes were not statistically significant. Interestingly, the induction of CYP3A4-specific catalytic activity in the duodenum of huCYP3A4/3A7 and huPXR/huCAR/huCYP3A4/3A7 mice treated with PCN or RIF, respectively, was more distinct and statistically significant. The reason for this difference in mRNA induction and increase in catalytic activity remains unknown. A possible explanation might be a difference in the kinetics of *CYP3A4* mRNA synthesis and degradation between the liver and the intestine so that the mRNA induction in the intestine is missed due to the timing of sample preparation. This explanation is also in agreement with a previous study in a PXR humanized mouse model which demonstrated that compared to the liver the intestinal CYP3A expression decreased more rapidly after withdrawal of RIF (Ma et al., 2007).

The absence of *CYP3A7* transcript in the liver and intestine of untreated huCYP3A4/3A7 and huPXR/huCAR/huCYP3A4/3A7 mice is in agreement with the classification of CYP3A7 as a fetally expressed CYP3A form, which is progressively lost after birth (Stevens et al., 2003). Interestingly, we found that *CYP3A7* mRNA expression can be induced to a limited extent in the liver of the adult CYP3A4/3A7 transgenic mice by PCN or RIF, respectively. This observation is in agreement with the previous identification of a functional PXR response element in the human *CYP3A7* promoter and with the transactivation of gene expression by

this element in response to PXR activators (Pascussi et al., 1999). Furthermore, our results support the potential PXR involvement in the expression of CYP3A7 which is observed occasionally in human liver (Burk et al., 2002). Nevertheless, it should be noted that the induced hepatic *CYP3A7* mRNA levels in the transgenic mice are more than three orders of magnitude lower than the induced *CYP3A4* levels in the corresponding animals and it is therefore unlikely that CYP3A7 contributes to the metabolism of the CYP3A4 probe substrates described in this work. Due to the fact that *CYP3A5* was not included in the targeting vector and 75% of Caucasians don't express CYP3A5, the huPXR/huCAR/huCYP3A4/3A7 model represents the majority of this group of the human population. However, it should be noted that in other ethnic groups, such as African Americans, CYP3A5 is expressed in a larger proportion of the population, which might not be accurately represented by the model.

In summary, the present paper describes the generation and characterization of a novel CYP3A4 humanized mouse line that was combined with a humanization of PXR and CAR. We provide evidence that this huPXR/huCAR/huCYP3A4/3A7 model can be a useful tool to rank different PXR activators according to their potency of inducing CYP3A4 in humans and to quantitatively predict PXR/CYP3A4-mediated drug-drug interactions in the clinic. Studies to establish whether the model can be used to evaluate CYP3A4/CAR interactions are the subject of further investigations. This model adds an important additional dimension to in vitro studies by allowing the assessment of induction responses on the basis of the pharmacokinetic changes of PXR activators in vivo. Furthermore, it offers the potential of studying the effects of compounds on both CYP3A4 induction and inhibition in an integrated single model system. The huPXR/huCAR/huCYP3A4/3A7 mouse line therefore might provide a valuable adjunct in existing technologies and in the design of clinical trials in man.

Molecular Pharmacology Fast Forward. Published on May 31, 2011 as DOI: 10.1124/mol.111.071845
This article has not been copyedited and formatted. The final version may differ from this version.

Acknowledgements

We wish to Anja Müller and Oliver Dahlmann (TaconicArtemis) for technical advice.

Molecular Pharmacology Fast Forward. Published on May 31, 2011 as DOI: 10.1124/mol.111.071845
This article has not been copyedited and formatted. The final version may differ from this version.

Authorship Contributions

Participated in research design: Hasegawa, Kapelyukh, Tahara, Seibler, Wolf, Scheer

Conducted experiments: Hasegawa, Kapelyukh, Rode, Krueger, Lee

Performed data analysis: Hasegawa, Kapelyukh, Tahara, Wolf, Scheer

Wrote or contributed to the writing of the manuscript: Hasegawa, Tahara, Wolf, Scheer

.

Molecular Pharmacology Fast Forward. Published on May 31, 2011 as DOI: 10.1124/mol.111.071845
This article has not been copyedited and formatted. The final version may differ from this version.

References

Anakk S, Kalsotra A, Kikuta Y, Huang W, Zhang J, Staudinger JL, Moore DD and Strobel HW (2004) CAR/PXR provide directives for Cyp3a41 gene regulation differently from Cyp3a11. *Pharmacogenomics J* **4**(2):91-101.

Backman JT, Olkkola KT and Neuvonen PJ (1996) Rifampin drastically reduces plasma concentrations and effects of oral midazolam. *Clin Pharmacol Ther* **59**(1):7-13.

Bradbrook ID, John VA, Morrison PJ, Rogers HJ and Spector RG (1982) Pharmacokinetics of single doses of sulphinpyrazone and its major metabolites in plasma and urine. *Br J Clin Pharmacol* **13**(2):177-185.

Budde K, Neumayer HH, Fritsche L, Sulowicz W, Stompor T and Eckland D (2003) The pharmacokinetics of pioglitazone in patients with impaired renal function. *Br J Clin Pharmacol* **55**(4):368-374.

Burk O, Tegude H, Koch I, Hustert E, Wolbold R, Glaeser H, Klein K, Fromm MF, Nuessler AK, Neuhaus P, Zanger UM, Eichelbaum M and Wojnowski L (2002) Molecular mechanisms of polymorphic CYP3A7 expression in adult human liver and intestine. *J Biol Chem* **277**(27):24280-24288.

Caforio AL, Gambino A, Tona F, Feltrin G, Marchini F, Pompei E, Testolin L, Angelini A, Dalla Volta S and Casarotto D (2000) Sulfinpyrazone reduces cyclosporine levels: a new drug interaction in heart transplant recipients. *J Heart Lung Transplant* **19**(12):1205-1208.

Cheung C and Gonzalez FJ (2008) Humanized mouse lines and their application for prediction of human drug metabolism and toxicological risk assessment. *J Pharmacol Exp Ther* **327**(2):288-299.

Chung E, Nafziger AN, Kazierad DJ and Bertino JS, Jr. (2006) Comparison of midazolam and simvastatin as cytochrome P450 3A probes. *Clin Pharmacol Ther* **79**(4):350-361.

Dai D, Bai R, Hodgson E and Rose RL (2001) Cloning, sequencing, heterologous expression, and characterization of murine cytochrome P450 3a25*(Cyp3a25), a testosterone 6beta-hydroxylase. *J Biochem Mol Toxicol* **15**(2):90-99.

de Wildt SN, Kearns GL, Leeder JS and van den Anker JN (1999) Cytochrome P450 3A: ontogeny and drug disposition. *Clin Pharmacokinet* **37**(6):485-505.

Fahmi OA, Hurst S, Plowchalk D, Cook J, Guo F, Youdim K, Dickins M, Phipps A, Darekar A, Hyland R and Obach RS (2009) Comparison of different algorithms for predicting clinical drug-drug interactions, based on the use of CYP3A4 in vitro data: predictions of compounds as precipitants of interaction. *Drug Metab Dispos* **37**(8):1658-1666.

Forrester LM, Neal GE, Judah DJ, Glancey MJ and Wolf CR (1990) Evidence for involvement of multiple forms of cytochrome P-450 in aflatoxin B1 metabolism in human liver. *Proc Natl Acad Sci U S A* **87**(21):8306-8310.

Granvil CP, Yu AM, Elizondo G, Akiyama TE, Cheung C, Feigenbaum L, Krausz KW and Gonzalez FJ (2003) Expression of the human CYP3A4 gene in the small intestine of transgenic mice: in vitro metabolism and pharmacokinetics of midazolam. *Drug Metab Dispos* **31**(5):548-558.

Hebert MF, Roberts JP, Prueksaritanont T and Benet LZ (1992) Bioavailability of cyclosporine with concomitant rifampin administration is markedly less than predicted by hepatic enzyme induction. *Clin Pharmacol Ther* **52**(5):453-457.

Hogan BLM, Beddington RSP, Costantini F and Lacy E (1994) in *Manipulating the Mouse Embryo: A Laboratory Manual* pp 253-289, Cold Spring Harbor Lab. Press, Plainview, New York.

Itoh S, Satoh M, Abe Y, Hashimoto H, Yanagimoto T and Kamataki T (1994) A novel form of mouse cytochrome P450 3A (Cyp3a-16). Its cDNA cloning and expression in fetal liver. *Eur J Biochem* **226**(3):877-882.

Kim S, Dinchuk JE, Anthony MN, Orcutt T, Zoeckler ME, Sauer MB, Mosure KW, Vuppugalla R, Grace JE, Jr., Simmermacher J, Dulac HA, Pizzano J and Sinz M (2010) Evaluation of cynomolgus monkey pregnane X receptor, primary hepatocyte, and in vivo pharmacokinetic changes in predicting human CYP3A4 induction. *Drug Metab Dispos* **38**(1):16-24.

Kim S, Pray D, Zheng M, Morgan DG, Pizzano JG, Zoeckler ME, Chimalakonda A and Sinz MW (2008) Quantitative relationship between rifampicin exposure and induction of Cyp3a11 in SXR humanized mice: extrapolation to human CYP3A4 induction potential. *Drug Metab Lett* **2**(3):169-175.

Kuehl P, Zhang J, Lin Y, Lamba J, Assem M, Schuetz J, Watkins PB, Daly A, Wrighton SA, Hall SD, Maurel P, Relling M, Brimer C, Yasuda K, Venkataramanan R, Strom S, Thummel K, Boguski MS and Schuetz E (2001) Sequence diversity in CYP3A promoters and characterization of the genetic basis of polymorphic CYP3A5 expression. *Nat Genet* **27**(4):383-391.

Kyrklund C, Backman JT, Kivisto KT, Neuvonen M, Laitila J and Neuvonen PJ (2000) Rifampin greatly reduces plasma simvastatin and simvastatin acid concentrations. *Clin Pharmacol Ther* **68**(6):592-597.

Lee G and Saito I (1998) Role of nucleotide sequences of loxP spacer region in Cre-mediated recombination. *Gene* **216**(1):55-65.

Ma X, Cheung C, Krausz KW, Shah YM, Wang T, Idle JR and Gonzalez FJ (2008) A double transgenic mouse model expressing human pregnane X receptor and cytochrome P450 3A4. *Drug Metab Dispos* **36**(12):2506-2512.

Ma X, Shah Y, Cheung C, Guo GL, Feigenbaum L, Krausz KW, Idle JR and Gonzalez FJ (2007) The PREgnane X receptor gene-humanized mouse: a model for investigating drug-drug interactions mediated by cytochromes P450 3A. *Drug Metab Dispos* **35**(2):194-200.

Moore LB, Parks DJ, Jones SA, Bledsoe RK, Consler TG, Stimmel JB, Goodwin B, Liddle C, Blanchard SG, Willson TM, Collins JL and Kliewer SA (2000) Orphan nuclear receptors constitutive androstane receptor and pregnane X receptor share xenobiotic and steroid ligands. *J Biol Chem* **275**(20):15122-15127.

Nebert DW and Russell DW (2002) Clinical importance of the cytochromes P450. *Lancet* **360**(9340):1155-1162.

Nelson DR, Zeldin DC, Hoffman SM, Maltais LJ, Wain HM and Nebert DW (2004) Comparison of cytochrome P450 (CYP) genes from the mouse and human genomes, including nomenclature recommendations for genes, pseudogenes and alternative-splice variants. *Pharmacogenetics* **14**(1):1-18.

Pascussi JM, Jounaidi Y, Drocourt L, Domergue J, Balabaud C, Maurel P and Vilarem MJ (1999) Evidence for the presence of a functional pregnane X receptor response element in the CYP3A7 promoter gene. *Biochem Biophys Res Commun* **260**(2):377-381.

Polk RE, Brophy DF, Israel DS, Patron R, Sadler BM, Chittick GE, Symonds WT, Lou Y, Kristoff D and Stein DS (2001) Pharmacokinetic Interaction between amprenavir and rifabutin or rifampin in healthy males. *Antimicrob Agents Chemother* **45**(2):502-508.

Prueksaritanont T, Vega JM, Zhao J, Gagliano K, Kuznetsova O, Musser B, Amin RD, Liu L, Roadcap BA, Dilzer S, Lasseter KC and Rogers JD (2001) Interactions between simvastatin and troglitazone or pioglitazone in healthy subjects. *J Clin Pharmacol* **41**(5):573-581.

Ripp SL, Mills JB, Fahmi OA, Trevena KA, Liras JL, Maurer TS and de Morais SM (2006) Use of immortalized human hepatocytes to predict the magnitude of clinical drug-drug interactions caused by CYP3A4 induction. *Drug Metab Dispos* **34**(10):1742-1748.

Sahi J, Black CB, Hamilton GA, Zheng X, Jolley S, Rose KA, Gilbert D, LeCluyse EL and Sinz MW (2003) Comparative effects of thiazolidinediones on in vitro P450 enzyme induction and inhibition. *Drug Metab Dispos* **31**(4):439-446.

Sakuma T, Takai M, Endo Y, Kuroiwa M, Ohara A, Jarukamjorn K, Honma R and Nemoto N (2000) A novel female-specific member of the CYP3A gene subfamily in the mouse liver. *Arch Biochem Biophys* **377**(1):153-162.

Scheer N, Ross J, Kapelyukh Y, Rode A and Wolf CR (2010) In vivo responses of the human and murine pregnane X receptor to dexamethasone in mice. *Drug Metab Dispos* **38**(7):1046-1053.

Scheer N, Ross J, Rode A, Zevnik B, Niehaves S, Faust N and Wolf CR (2008) A novel panel of mouse models to evaluate the role of human pregnane X receptor and constitutive androstane receptor in drug response. *J Clin Invest* **118**(9):3228-3239.

Schlicht F, Staiger C, de Vries J, Gundert-Remy U, Hildebrandt R, Harenberg J, Wang NS and Weber E (1985) Pharmacokinetics of sulphinpyrazone and its major metabolites after a single dose and during chronic treatment. *Eur J Clin Pharmacol* **28**(1):97-103.

Sinz M, Kim S, Zhu Z, Chen T, Anthony M, Dickinson K and Rodrigues AD (2006) Evaluation of 170 xenobiotics as transactivators of human pregnane X receptor (hPXR) and correlation to known CYP3A4 drug interactions. *Curr Drug Metab* **7**(4):375-388.

Stanley LA, Horsburgh BC, Ross J, Scheer N and Wolf CR (2006) PXR and CAR: nuclear receptors which play a pivotal role in drug disposition and chemical toxicity. *Drug Metab Rev* **38**(3):515-597.

Stevens JC, Hines RN, Gu C, Koukouritaki SB, Manro JR, Tandler PJ and Zaya MJ (2003) Developmental expression of the major human hepatic CYP3A enzymes. *J Pharmacol Exp Ther* **307**(2):573-582.

Tornio A, Niemi M, Neuvonen PJ and Backman JT (2008) Trimethoprim and the CYP2C8*3 allele have opposite effects on the pharmacokinetics of pioglitazone. *Drug Metab Dispos* **36**(1):73-80.

van Herwaarden AE, Wagenaar E, van der Kruijssen CM, van Waterschoot RA, Smit JW, Song JY, van der Valk MA, van Tellingen O, van der Hoorn JW, Rosing H, Beijnen JH and Schinkel AH (2007) Knockout of cytochrome P450 3A yields new mouse models for understanding xenobiotic metabolism. *J Clin Invest* **117**(11):3583-3592.

Villikka K, Kivisto KT, Backman JT, Olkkola KT and Neuvonen PJ (1997) Triazolam is ineffective in patients taking rifampin. *Clin Pharmacol Ther* **61**(1):8-14.

Wallace HA, Marques-Kranc F, Richardson M, Luna-Crespo F, Sharpe JA, Hughes J, Wood WG, Higgs DR and Smith AJ (2007) Manipulating the mouse genome to engineer precise functional syntenic replacements with human sequence. *Cell* **128**(1):197-209.

Williams JA, Ring BJ, Cantrell VE, Jones DR, Eckstein J, Ruterbories K, Hamman MA, Hall SD and Wrighton SA (2002) Comparative metabolic capabilities of CYP3A4, CYP3A5, and CYP3A7. *Drug Metab Dispos* **30**(8):883-891.

Xie W, Barwick JL, Downes M, Blumberg B, Simon CM, Nelson MC, Neuschwander-Tetri BA, Brunt EM, Guzelian PS and Evans RM (2000) Humanized xenobiotic response in mice expressing nuclear receptor SXR. *Nature* **406**(6794):435-439.

Yanagimoto T, Itoh S, Sawada M and Kamataki T (1997) Mouse cytochrome P450 (Cyp3a11): predominant expression in liver and capacity to activate aflatoxin B1. *Arch Biochem Biophys* **340**(2):215-218.

Yu AM, Fukamachi K, Krausz KW, Cheung C and Gonzalez FJ (2005) Potential role for human cytochrome P450 3A4 in estradiol homeostasis. *Endocrinology* **146**(7):2911-2919.

Zhang J, Huang W, Chua SS, Wei P and Moore DD (2002) Modulation of acetaminophen-induced hepatotoxicity by the xenobiotic receptor CAR. *Science* **298**(5592):422-424.

Molecular Pharmacology Fast Forward. Published on May 31, 2011 as DOI: 10.1124/mol.111.071845
This article has not been copyedited and formatted. The final version may differ from this version.

Footnotes

Financial support:

Part of this work was supported by ITI Life Sciences, Scotland.

Joint authorships

Joint first author (MH, YK)

Joint last author (CRW, NS)

Reprint requests:

Nico Scheer, PhD, TaconicArtemis, Neurather Ring 1, 51063 Koeln, Germany.

Tel.: +49 221 9645343; Fax: +49 221 9645321; Email: nico.scheer@taconicartemis.com

Molecular Pharmacology Fast Forward. Published on May 31, 2011 as DOI: 10.1124/mol.111.071845
This article has not been copyedited and formatted. The final version may differ from this version.

Figure Legends

Fig. 1. Strategy to generate Cyp3a$^{-/-}$/Cyp3a13$^{+/+}$ and huCYP3A4/3A7 mice. (A) Schematic representation of the chromosomal organization and orientation of functional genes within the mouse *Cyp3a* Cluster. Pseudogenes are not listed. (B) Exon/Intron structure of *Cyp3a57* and *Cyp3a59*. Exons are represented as black bars and the ATGs mark the translational start sites of both genes. The positions of the targeting arms for homologous recombination are highlighted as light (*Cyp3a57*) and dark (*Cyp3a59*) grey lines, respectively. (C) Vectors used for targeting of *Cyp3a57* (left) and *Cyp3a59* (right) by homologous recombination. (D) Genomic organization of the *Cyp3a* Cluster in double targeted ES cells after homologous recombination on the same allele at the *Cyp3a57* and *Cyp3a59* locus. (E) Deletion of the mouse *Cyp3a* Cluster after *Cre*-mediated recombination at the *loxP* sites. (F) Modified human BAC containing *CYP3A4* and *CYP3A7* used for Cre-mediated insertion into the *loxP* and *lox5171* sites of the prepared *Cyp3a* knockout locus. (G) Targeted mouse *Cyp3a* locus after Cre-mediated recombination of the modified human BAC into the *loxP* and *lox5171* sites of the *Cyp3a* knockout allele. (H) Humanized *Cyp3a* locus after Flp-mediated deletion of the *frt* and *f3*-flanked Hygromycin and Neomycin expression cassettes. The ES cells shown in (E) and (H) were used to generate the Cyp3a$^{-/-}$/Cyp3a13$^{+/+}$ and huCYP3A4/3A7 mice, respectively, as described in the Methods section. For the sake of clarity sequences are not drawn to scale. *LoxP* , *lox5171*, *frt* and *f3* sites are represented as white, striped, black or grey triangles, respectively. TK = Thymidine Kinase expression cassette, Hygro = Hygromycine expression cassette, ZsGreen = ZsGreen expression cassette, P = Promoter that drives the expression of Neomycin, 5'Δ Neo = ATG-deficient Neomycin.

Molecular Pharmacology Fast Forward. Published on May 31, 2011 as DOI: 10.1124/mol.111.071845
This article has not been copyedited and formatted. The final version may differ from this version.

Fig. 2. CYP3A4 mRNA and protein expression levels in the liver and duodenum of huCYP3A4/3A7 and huPXR/huCAR/huCYP3A4/3A7 mice. Relative quantification of *CYP3A4* mRNA in (A) liver and (B) duodenum samples from huCYP3A4/3A7 and huPXR/huCAR/hCYP3A4/3A7 mice treated by i.p. injection with either corn oil, RIF (10 mg/kg daily for 3 days) or PCN (10mg/kg daily for 2 days). The *CYP3A4* expression level in corn oil treated huPXR/huCAR/huCYP3A4/3A7 mice was arbitrarily set as one. Data are expressed as Mean ± SD. The *CYP3A4* mRNA level of samples from treated mice was compared to that from the corresponding control group with a Student's t-test (2-sided), with * and ** statistically different from control at $p<0.05$, <0.01 and <0.001, respectively. CYP3A4 protein expression in (C) liver and (D) intestinal microsomes from huCYP3A4/3A7 and huPXR/huCAR/huCYP3A4/3A7 mice receiving the same treatment as described above. Each lane is a sample from pooled microsomes. 3 μg of protein were loaded for each sample. Blots were incubated in a polyclonal rabbit anti-CYP3A4 (Gentest, cat # 458234). Positive controls: Recombinant human CYP3A4 (Invitrogen P2377, 0.02 pmol loaded), single donor human liver microsomes (CellzDirect, HMMC-SD-118 and HMMC-SD-002, 3μg loaded) and pooled human liver microsomes (pHLM, BD Biosciences 452161, 3μg loaded). In all cases n=3 for huCYP3A4/3A7 and n=2 for huPXR/huCAR/huCYP3A4/3A7 mice.

Fig. 3. Oxidation of CYP3A4 probe substrates by liver and intestinal microsomes from huCYP3A4/3A7, huPXR/huCAR/huCYP3A4/3A7 and Cyp3a$^{-/-}$/3a13$^{+/+}$ mice. TRZ, DBF and MDZ oxidation by (A) liver and (B) intestinal microsomes from huCYP3A4/3A7, huPXR/huCAR/hCYP3A4/3A7 and Cyp3a$^{-/-}$/3a13$^{+/+}$ mice treated by i.p. injection with either corn oil, RIF (10mg/kg daily for 3 days) or PCN (10mg/kg daily for 2 days) was measured by the formation of the corresponding metabolites. Data are expressed as Mean ± SD (n=3 mice for huCYP3A4/3A7 liver and intestinal microsomes and Cyp3a$^{-/-}$/3a13$^{+/+}$intestinal microsomes, n=1 mouse for Cyp3a$^{-/-}$/3a13$^{+/+}$ liver microsomes and n=2 mice for

huPXR/huCAR/hCYP3A4/3A7 liver and intestinal microsomes). Activities of samples from treated mice were compared to that from the corresponding control group with a Student's t-test (2-sided), with *, ** and *** statistically different from control at $p<0.05$, <0.01 and <0.001, respectively.

Fig. 4. Plasma concentration-time curves for different doses of rifampicin, sulfinpyrazone and pioglitazone in huPXR/huCAR/huCYP3A4/3A7 mice. Plasma concentration-time curves in huPXR/huCAR/huCYP3A4/3A7 mice given oral doses of 1, 3 or 10 mg/kg RIF (A), 0.5, 2 or 10 mg/kg SUL (B) or 2, 10 or 50 mg/kg PIO (C). Measurements for the lowest doses are indicated as circles, for medium dose as triangles and for highest dose as squares. Plasma concentration-time profiles at 4 hours after administration are compared for day one (closed symbol) and day four (open symbol). For the 2 mg/kg treatment group the PIO plasma concentration at 24 hrs was below the limit of detection. Each point represents the Mean ± SD (n=3 mice per compound and treatment).

Fig. 5. Relative expression of *CYP3A4* mRNA in the liver and intestine of huCYP3A4/3A7 and huPXR/huCAR/huCYP3A4/3A7 mice treated with rifampicin, sulfinpyrazone and pioglitazone. Total RNA was isolated from the liver (A) and intestine (B) of huCYP3A4/3A7 (closed bar) and huPXR/huCAR/huCYP3A4/3A7 (open bar) mice treated with different doses of RIF, SUL and PIO (n=3 mice per genotype, compound and treatment). Values represent the mean expression level ± SD relative to the vehicle treated control group. The *CYP3A4* mRNA expression levels were normalized to murine β-actin. One-way analysis of variance with Dunnett test or student's t-test was performed on the results; with *, ** and *** statistically different from control at $p<0.05$, <0.01 and <0.001, respectively.

Molecular Pharmacology Fast Forward. Published on May 31, 2011 as DOI: 10.1124/mol.111.071845
This article has not been copyedited and formatted. The final version may differ from this version.

Fig. 6. Triazolam plasma concentration-time curves following different doses of rifampicin, sulfinpyrazone and pioglitazone in huPXR/huCAR/huCYP3A4/3A7 mice. TRZ plasma concentration-time curves in huPXR/huCAR/huCYP3A4/3A7 mice given oral doses of 1, 3 or 10 mg/kg RIF (A), 0.5, 2 or 10 mg/kg SUL (B) or 2, 10 or 50 mg/kg PIO (C) and followed by a 5 mg/kg oral dose of TRZ. Measurements for the vehicle are indicated as open circles, for the lowest doses as closed circles, for medium dose as closed triangles and for highest dose as closed squares. Each point represents the Mean ± SD (n=3 mice per compound and treatment).

Molecular Pharmacology Fast Forward. Published on May 31, 2011 as DOI: 10.1124/mol.111.071845
This article has not been copyedited and formatted. The final version may differ from this version.

Tables

TABLE 1

Pharmacokinetic parameters for different doses of rifampicin, sulfinpyrazone and pioglitazone in huPXR/huCAR/huCYP3A4/3A7 mice.

Data represent the Mean ± SD (n=3 mice per compound and treatment).

	Dose (mg/kg)	t_{max} (h)	C_{max} (ng/ml)	$t_{1/2}$ (h)	$AUC_{0-\infty}$ (ng x h/ml)
Rifampicin	1	1.3 ± 0.6	453 ± 60	8.17 ± 1.46	5920 ± 530
	3	0.7 ± 0.3	2220 ± 230	6.18 ± 2.14	21500 ± 1800
	10	1.2 ± 0.8	17600 ± 7800	6.46 ± 1.35	124000 ± 4000
Sulfinpyrazone	0.5	1.0 ± 0.9	1770 ± 1540	6.12 ± 0.39	10400 ± 1800
	2	0.5 ± 0.0	4250 ± 380	7.11 ± 0.97	43200 ± 8700
	10	1.0 ± 0.0	31500 ± 8700	7.92 ± 1.19	230000 ± 131000
Pioglitazone	2	0.8 ± 0.3	2680 ± 340	2.54 ± 1.67	11400 ± 2400
	10	0.7 ± 0.3	8460 ± 810	2.20 ± 0.13	52900 ± 5700
	50	1.0 ± 0.9	37100 ± 7700	2.37 ± 0.26	154000 ± 25000

Molecular Pharmacology Fast Forward. Published on May 31, 2011 as DOI: 10.1124/mol.111.071845
This article has not been copyedited and formatted. The final version may differ from this version.

TABLE 2

Pharmacokinetic parameters of triazolam for different doses of rifampicin, sulfinpyrazone and pioglitazone in huPXR/huCAR/huCYP3A4/3A7 mice.

huPXR/huCAR/huCYP3A4/3A7 mice were given different oral doses of RIF, SUL or PIO followed by a 5 mg/kg oral dose of TRZ. Data represent the Mean ± SD (n=3 mice per compound and treatment). The TRZ C_{max} and AUC values from mice treated with RIF, SUL or PIO were compared to those from the corresponding vehicle treated control group with a one-way analysis of variance with Dunnett test, with * and ** statistically different from control at $p<0.05$ and <0.01, respectively.

	Dose (mg/kg)	TRZ t_{max} (h)	TRZ C_{max} (ng/ml)	TRZ $t_{1/2}$ (h)	TRZ $AUC_{0-\infty}$ (ng x h/ml)	TRZ AUC decrease (%)
Rifampicin	0	1.0 ± 0.0	730 ± 341	1.26 ± 0.38	1680 ± 580	-
	1	0.5 ± 0.0	464 ± 181	1.01 ± 0.17	814 ± 356	52
	3	0.5 ± 0.0	337 ± 131	1.49 ± 0.27	615 ± 315*	63
	10	0.5 ± 0.0	113 ± 23*	1.23 ± 0.22	156 ± 11**	91
Sulfinpyrazone	0	0.5 ± 0.0	484 ± 93	1.39 ± 0.31	1200 ± 240	-
	0.5	0.7 ± 0.3	467 ± 109	1.46 ± 0.31	1190 ± 180	1
	2	0.5 ± 0.0	447 ± 104	1.28 ± 0.25	1020 ± 230	15
	10	0.5 ± 0.0	351 ± 49	1.43 ± 0.26	756 ± 71*	37
Pioglitazone	0	0.7 ± 0.3	624 ± 124	1.31 ± 0.31	1420 ± 240	-
	2	0.5 ± 0.0	653 ± 163	1.15 ± 0.12	1390 ± 340	2
	10	0.8 ± 0.3	767 ± 176	1.06 ± 0.03	1420 ± 390	0
	50	0.5 ± 0.0	906 ± 90	1.20 ± 0.17	1890 ± 450	-33

Figure 1

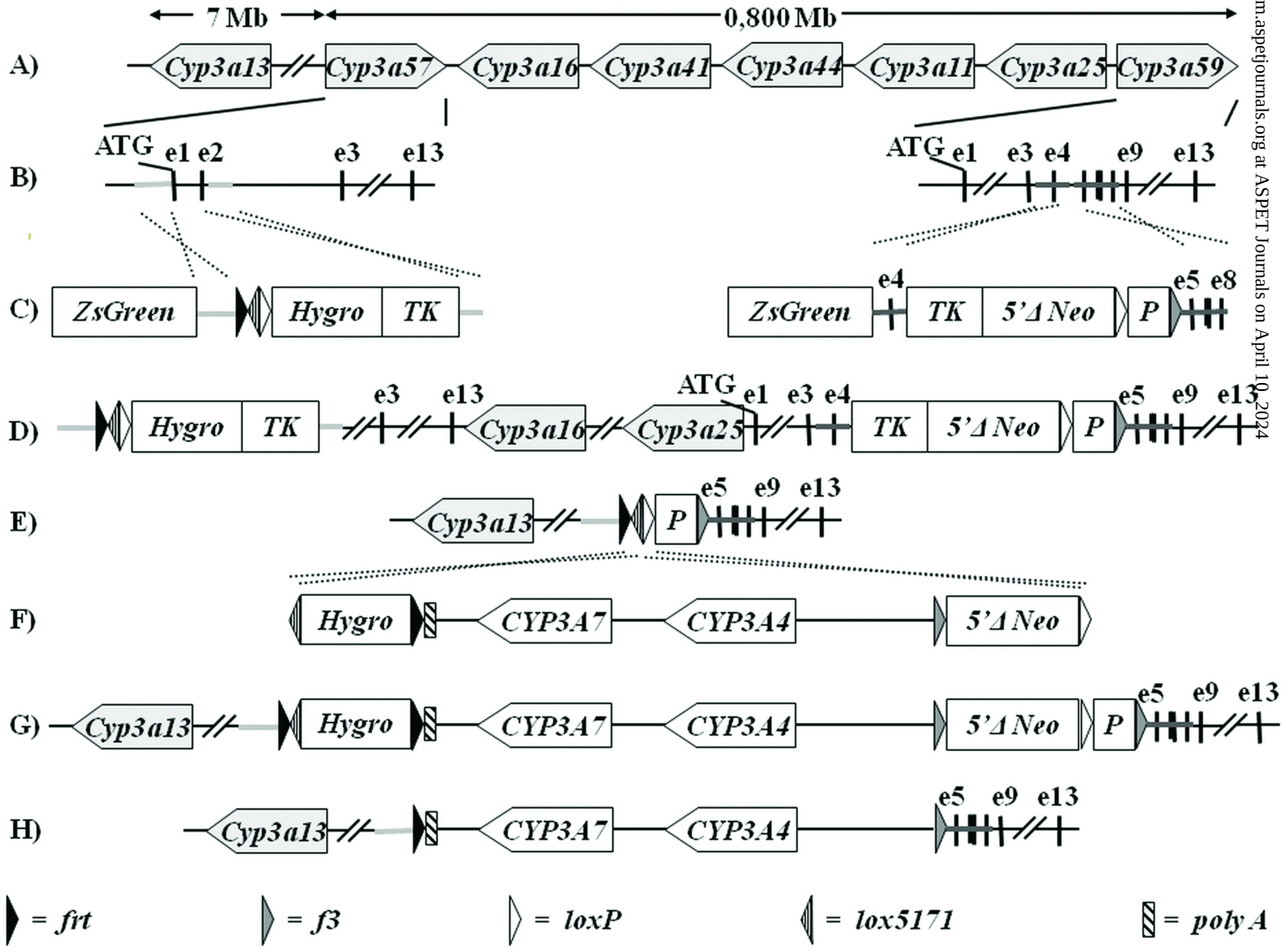

Figure 2

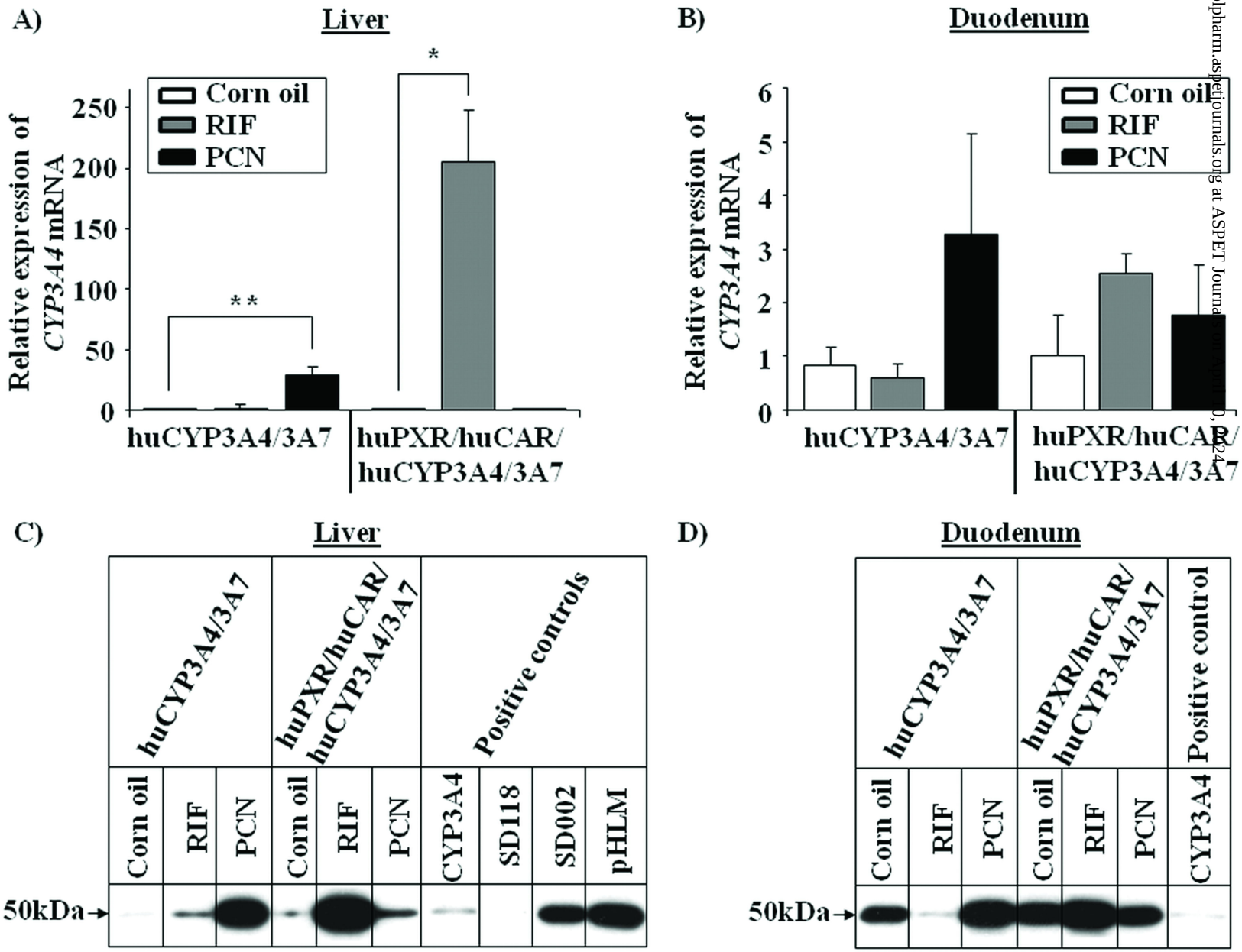

Figure 3

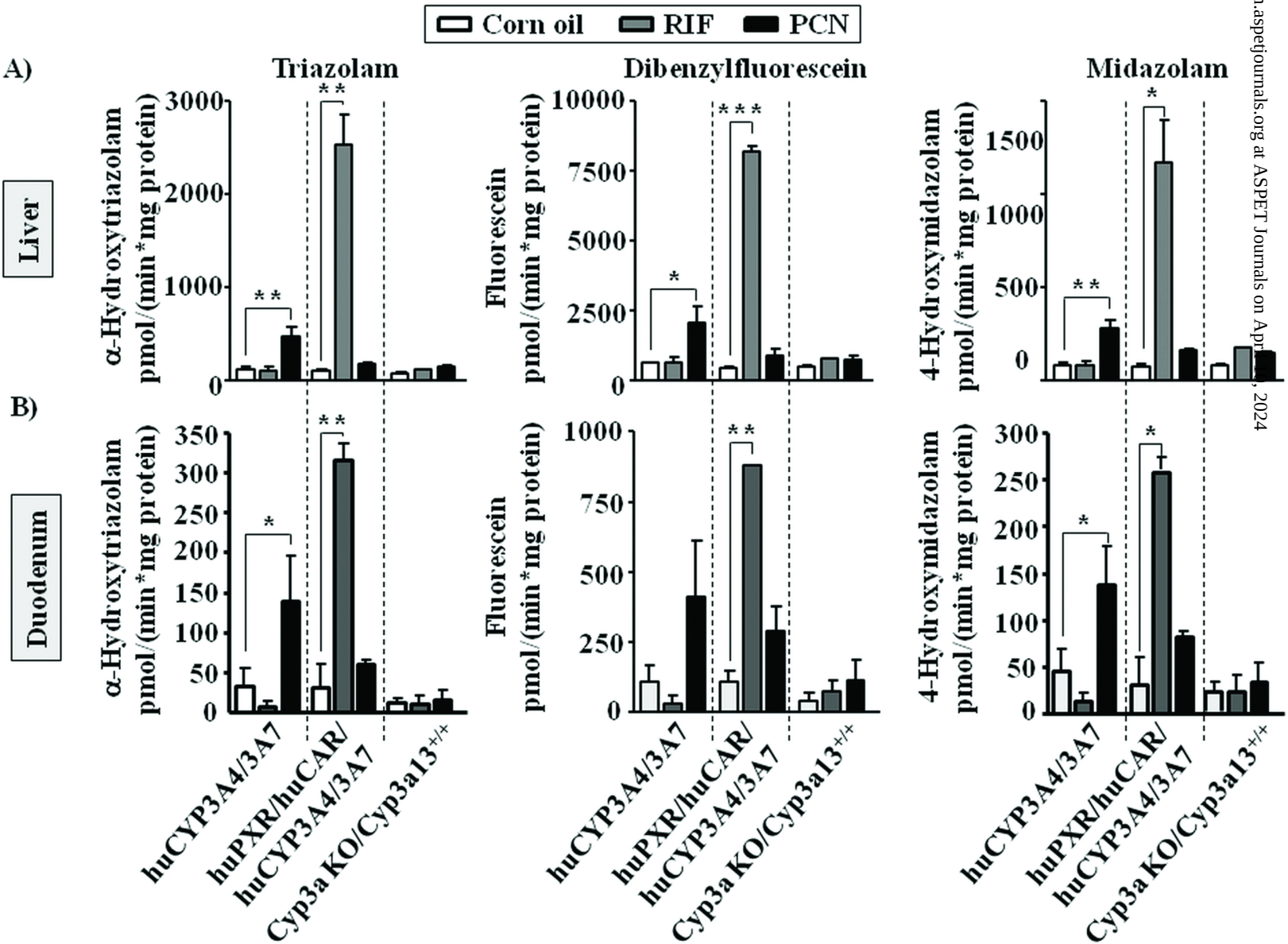

Figure 4

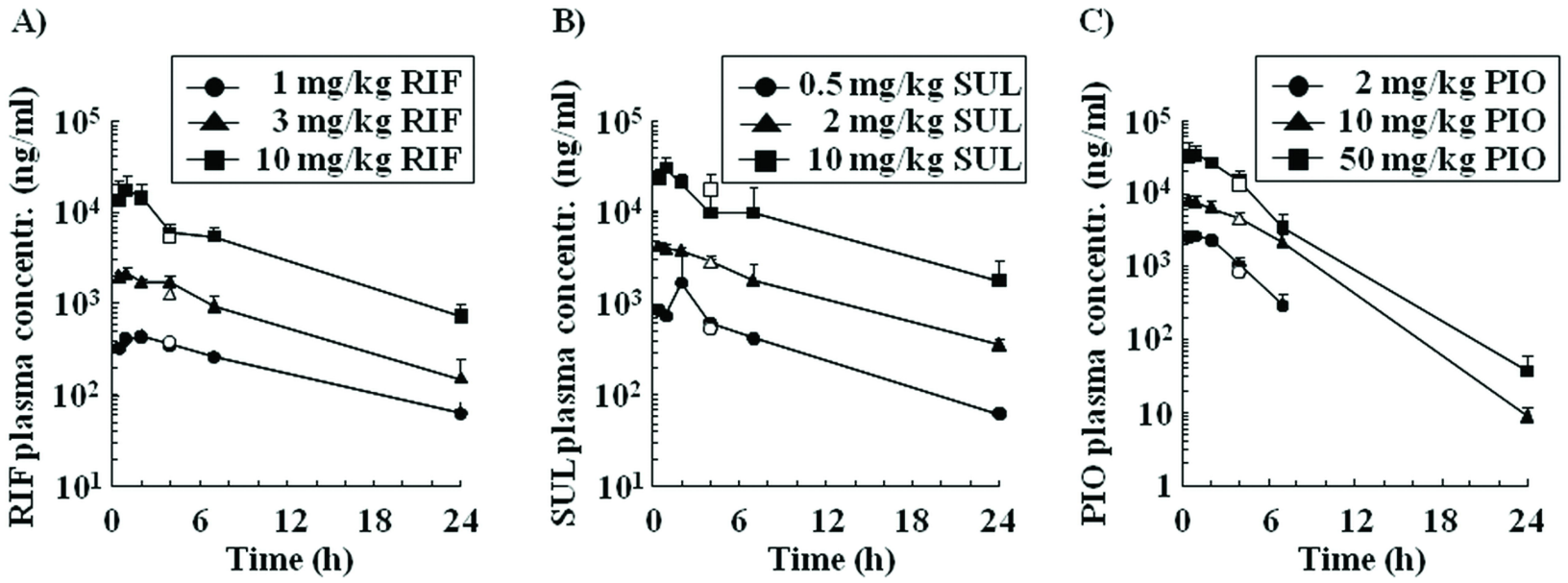
A)
1 mg/kg RIF
3 mg/kg RIF
10 mg/kg RIF
RIF plasma concentr. (ng/ml)
Time (h)
B)
0.5 mg/kg SUL
2 mg/kg SUL
10 mg/kg SUL
SUL plasma concentr. (ng/ml)
Time (h)
C)
2 mg/kg PIO
10 mg/kg PIO
50 mg/kg PIO
PIO plasma concentr. (ng/ml)
Time (h)

Figure 5

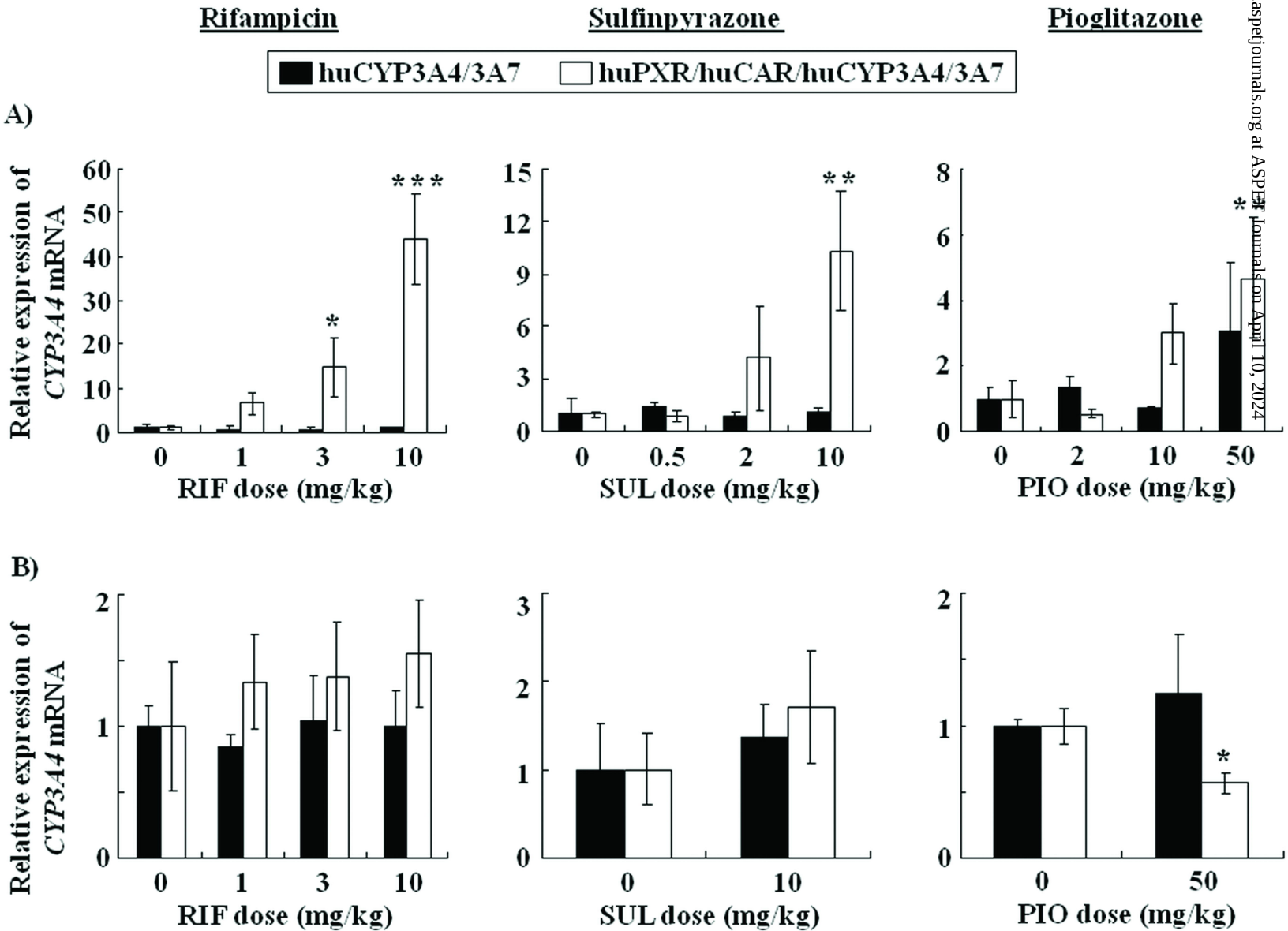

Figure 6

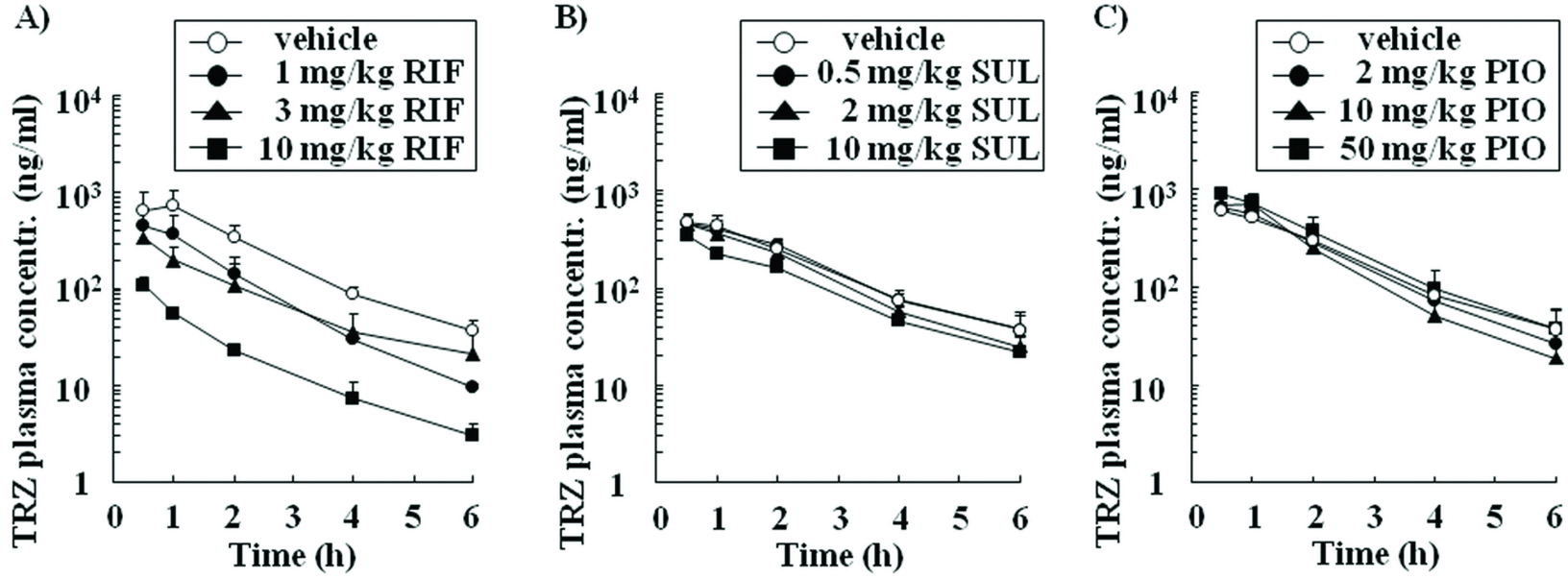
A)
vehicle
1 mg/kg RIF
3 mg/kg RIF
10 mg/kg RIF
TRZ plasma concentr. (ng/ml)
Time (h)
B)
vehicle
0.5 mg/kg SUL
2 mg/kg SUL
10 mg/kg SUL
TRZ plasma concentr. (ng/ml)
Time (h)
C)
vehicle
2 mg/kg PIO
10 mg/kg PIO
50 mg/kg PIO
TRZ plasma concentr. (ng/ml)
Time (h)

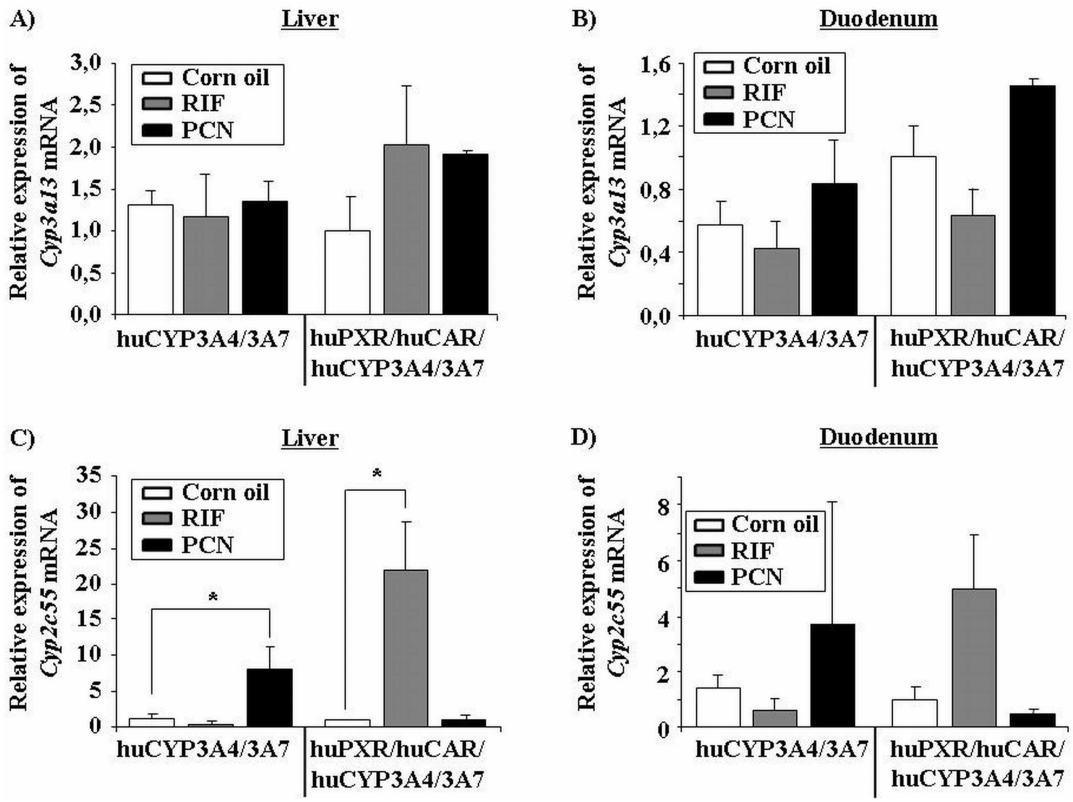

Supplementary Fig. 1. *Cyp3a11* and *Cyp2c55* mRNA expression levels in the liver and duodenum of huCYP3A4/3A7 and huPXR/huCAR/huCYP3A4/3A7 mice. Relative quantification of *Cyp3a11* mRNA in (*A*) liver and (*B*) duodenum and of *Cyp2c55* mRNA in (*C*) liver and (*D*) duodenum from huCYP3A4/3A7 and huPXR/huCAR/hCYP3A4/3A7 mice treated by i.p. injection with either corn oil, RIF (10 mg/kg daily for 3 days) or PCN (10 mg/kg daily for 2 days). The *Cyp3a11* and *Cyp2c55* expression levels in corn oil treated huPXR/huCAR/huCYP3A4/3A7 mice were arbitrarily set as one. Data are expressed as Mean ± SD (n=3 for huCYP3A4/3A7 and n=2 for huPXR/huCAR/huCYP3A4/3A7 mice). The mRNA levels of samples from treated mice were compared to those from the corresponding control group with a Student's t-test (2-sided), with * statistically different from control at $p<0.05$.

Supplementary Materials and Methods

Vector construction and ES cell targeting to generate Cyp3a$^{-/-}$/Cyp3a13$^{+/+}$ and huCYP3A4/3A7 mice. First a basic vector for targeting the mouse *Cyp3a57* locus containing a Hygromycin, Thymidine Kinase and ZsGreen expression cassette, and a *loxP*, *lox5171* and *frt* site was constructed in pBluescript. A 5.5 kb genomic sequence immediately upstream of the translational start site of the mouse *Cyp3a57* gene and a 3.3 kb fragment located within intron 2 of *Cyp3a57*, both used as targeting arms for homologous recombination, were obtained by red/ET recombineering (56) and subcloned into the basic targeting vector as depicted in Fig. 1C. The targeting vector was linearized with NotI and electroporated into a C57BL/6 mouse ES cell line. Of 360 hygromycin resistant and fluorescence negative ES cell colonies screened by standard Southern blot analyses, 1 correctly targeted clone (B-G12) was identified, expanded and further analysed by Southern blot analyses with different suitable restriction enzymes and 5' and 3' external probes and an internal hygromycin probe. This clone was confirmed as correctly targeted at both homology arms and it didn't carry additional random integrations.

In order to generate double targeted ES cells in which the mouse *Cyp3a* cluster is flanked with *loxP* sites, a second vector for targeting the mouse *Cyp3a59* locus containing an ATG-deficient Neomycin (5'Δ Neo), a Thymidine Kinase and a ZsGreen expression cassette, and a *loxP* and *f3* site was constructed in pBluescript. The translational start ATG and the corresponding promoter is separated from the 5'Δ Neo cassette in frame by the *loxP* site, such that additional amino acids encoded by the *loxP* site are fused to the N-terminus of Neomycin giving rise to a functional protein resulting in G418 resistance upon expression. A 4.3 kb genomic sequence comprising exon 4 of the mouse *Cyp3a59* gene and a 5.8 kb fragment comprising exons 5-8 of *Cyp3a59*, both used as targeting arms for homologous

recombination, were obtained by red/ET recombineering and subcloned into the basic targeting vector as depicted in Fig. 1C. The targeting vector was linearized with NotI and electroporated into the correctly targeted *Cyp3a57* ES clones B-G12 described above. Of 271 G418 resistant and fluorescence negative ES cell colonies screened by standard Southern blot analyses, 1 correctly targeted clone (A-B5) was identified, expanded and further analysed by Southern blot analyses as described above. This clone was confirmed as correctly targeted at both homology arms and it didn't carry additional random integrations.

For Cre-mediated deletion of the *Cyp3a* Cluster in the double targeted ES cells, 1 x 10^7 ES cells derived from clone A-B5 (see above) were electroporated with the Cre-expression plasmid pCAGGScrepA as previously described (57) and were plated at 1 and 5 x 10^5 cells, respectively, on 10 cm dishes and selected wit 2 µM Ganciclovir (Merck KGaA, Darmstadt, Germany). Approximately 100 clones survived this selection, pointing to targeting of *Cyp3a57* and *Cyp3a59* on the same allele in clone A-B5 and a successful deletion of the mouse cluster as indicated by the loss of the TK-expression cassette conferring resistance to Ganciclovir. Resistant clones were transferred to individual wells of a 96-well plate, expanded and further analysed for deletion of the *Cyp3a* Cluster by PCR with the primers 5'-GACATTGACATCCACTTTGCC-3' and 5'- GGGAGGGAAACTTGGAGG-3'. Cre-mediated deletion of the *Cyp3a* Cluster brings these to primers in proximity on the chromosome giving rise to a 319 bp fragment by PCR. 7 of 8 Ganciclovir resistant ES cell clones analysed by PCR showed the expected band of 319 bps, confirming the successful deletion of the *Cyp3a* Cluster in those clones. *Cyp3a* deleted ES cell clones were used to generate Cyp3a$^{-/-}$/3a13$^{+/+}$ mice and were further modified by the insertion of a BAC carrying human *CYP3A4* and *CYP3A7* (see below).

In order to generate ES cell clones with a genomic swap of mouse *Cyp3a* with human *CYP3A* genes, the BAC clone RP11-757A13 (ImaGenes GmbH, Robert-Rössle-Str.10, 13125 Berlin, Germany, ImaGenes Clone ID: RPCIB753A13757Q) was modified by red/ET

recombineering, such that the existing *lox* sites in the BAC are replaced with appropriately located *loxP* and *lox5171* sites and a hygromycin and 5' deficient neomycin selection cassette are introduced (Fig. 1F). This allows the insertion of the modified BAC via Cre-mediated recombination at the corresponding *lox* sites in the prepared *Cyp3a* deleted ES cell clones (see above) and selection of correctly targeted clones with high stringency by the complementation of the deficient neomycin cassette with the promoter and ATG remaining at the deleted *Cyp3a* locus (Fig. 1G). In addition, the heterospecific flipase recombinase (Flp) recognition sites *frt* and *f3* were introduced into the BAC enabling the subsequent removal of the hygromycin and neomycin selection cassettes in vivo by Flp-mediated recombination (Fig. 1H) and a *polyA* motif was used to terminate any potential transcription initiated from the endogenous mouse *Cyp3a57* promoter, which has not been deleted.

Cyp3a-deleted subclones derived from the parental clone A-B5 (see above) were used to insert the modified BAC carrying human *CYP3A4* and *CYP3A7* by Cre-mediated recombination (Fig. 1F). For this purpose, $1x10^7$ cells were electroporated under standard conditions with approximately 30 µg of supercoiled BAC DNA and 12 µg of the Cre-expression plasmid pCAGGScrepA as previously described (57) and selected with G418. Seven G418 resistant ES cell clones were obtained after the electroporation procedure. Three of the clones were expanded and further analysed by PCR and Southern blot with different suitable restriction enzymes, 5′ and 3′ external probes, and an internal neomycin probe. All three clones were confirmed as correctly recombined at both *lox* sites, were shown to carry a single copy of the integrated BAC and didn't carry additional random integrations. In addition, the CYP3A4 exons in the ES cell clone used to generate huCYP3A4/3A7 mice were sequenced and it was verified that the coding region is in agreement with the accepted reference sequence (http://www.cypalleles.ki.se/cyp3a4.htm).

Quantification of rifampicin, sulfinpyrazone, pioglitazone and triazolam in plasma. For RIF the plasma samples were 5-fold diluted by mouse blank plasma. Two microliters of plasma, 23 µl of 10 mmol/l ammonium acetate, and 50 µl of ice-cold internal standard solution (acetonitrile, 0.2 µmol/l) were mixed and centrifuged (5000xg, 4°C, 10 min). Fifty microliters of the supernatant was mixed with 100 µl of 10 mmol/l ammonium acetate and the mixture was injected into a LC/MS/MS. For SUL and TRZ 2 µl of plasma, 2 µl of DMSO and 30 µl of the ice-cold internal standard solution (methanol, 0.2 µmol/l) were mixed and centrifuged (5000xg, 4°C, 10 min). Twenty microliters of the supernatant was mixed with 80 µl of 10 mmol/l ammonium acetate and the mixture was injected into a LC/MS/MS. For PIO the plasma samples were 5-fold diluted by mouse blank plasma. Two microliters of plasma, 2 µl of DMSO and 30 µl of ice-cold internal standard solution (methanol, 0.2 µmol/l) were mixed and centrifuged (5000xg, 4°C, 10 min). Twenty microliters of the supernatant was mixed with 80 µl of water containing 0.05% formic acid and the mixture was injected into a LC/MS/MS. Propranolol was used as the internal standard in the measurement of plasma concentrations of RIF, SUL, PIO and TRZ.

Chromatographic separation was performed on an ACQUITY UPLC BEH C18 column (1.7 µm, 2.1 mm I.D. x 50 mm) (Waters, Milford, MA) using an injection volume of 5 µl (RIF), 2.5 µl (SUL), 7.5 µl (PIO) and 10 µl (TRZ) and a run time of 2.5 minutes. Elution was conducted at a flow rate of 0.5 ml/min by a linear gradient with the mobile phase, which consisted of 10 mmol/l ammonium acetate in water (A for RIF, SUL and TRZ) or 0.05% formic acid in water (A for PIO) and methanol (B). Gradient conditions were as follows: At 0, 1.5 and 1.6 minutes, B% was 80, 5 and 80, respectively (RIF), at 0, 0.2, 1.5, 1.51, 2 and 2.01 minutes, B% was 80, 80, 20, 10, 10 and 80, respectively (SUL) and 70, 70, 20, 10, 10 and 70, respectively (PIO and TRZ). The detector used was a 4000 QTRAP AB SCIEX mass spectrometer (Applied Biosystems, Foster City, CA) run in electrospray positive ion mode. The multiple reaction monitoring parameters for RIF were 823.6 (Q1 mass) and 791.4 (Q3

mass), for SUL 405.0 and 279.4, for PIO 357.0 and 134.2, for TRZ 343.4 and 308.1, for 1-OH-TRZ 359.1 and 176.1 and for 4-OH-TRZ 359.1 and 314.1, respectively.

Quantitative Reverse Transcriptase PCR (qRT-PCR). In case of the data presented on Fig. 2, Supplementary Fig. 1 and Supplementary Table 2 cDNA was synthesized from 1µg total RNA using the QIAGEN Quantiscript Reverse Transcriptase Kit (Hilden, Germany). Primers used were from the following assay-on-demand kits; *CYP3A4* (Hs00604506_m1), *CYP3A7* (Hs00426361_m1), *Cyp3a13* (Mm00484110_m1), *Cyp2c55* (Mm00472168_m1) and *β-actin* (Mm00607939_m1) (Applied Biosystems, Foster City, CA). Quantitative RT-PCR reactions were performed using TaqMan Universal PCR Mastermix in an ABI PRISM 7000 Sequence Detection System (Applied Biosystems). In case of the data presented on Fig. 5 cDNA was synthesized by reverse transcription using PrimeScript RT reagent kit (TAKARA **Define!**). 100 ng of total RNA was added to 10 µL of a reaction mixture. The synthesized cDNA sample was 10-fold diluted by distilled water. SYBR® Green PCR was performed by ABI PRISM 7900HT (Applied Biosystems) using SYBR Premix Ex Taq (TAKARA). Twenty microliters of a reaction mixture contained 5 µL of diluted cDNA solution. Final primer concentration was 0.2 µmol/l. The PCR conditions were as follows: After initial denaturation at 94 °C for 5 min, the amplification was performed by denaturation at 94 °C for 30 s, annealing at 65 °C for 30 s and extension at 72 °C for 30 s for 45 cycles. The primer sequences for *CYP3A4* were 5'-AGTTAATCCACTGTGACTTTGCCC (forward) and 5'-TGAGGATGGAATGCAAGAGG (revers) and for *ß-actin* 5'- ACAGCTGAGAGGGAAATCG (forward) and 5'- AGTACTTGCGCTCAGGAGG (revers). Data were analysed using comparative cycling time methodology, in which fluorescent output, measured as Ct, was directly proportional to input cDNA concentration. Ct values >35 were interpreted as being at the limit of detection of the TaqMan and therefore not quantitatively analyzed. In all cases input

cDNA concentrations were normalized to murine β-actin (ΔCt). Where appropriate relative expression levels were compared by a $2(^{-\Delta\Delta Ct})$ calculation.

Measurement of TRZ, MDZ, DBF and testosterone oxidation in microsomes. DBF (2 µM) was incubated with 5 µl (final protein concentration approximately 0.075 mg/ml) liver or 25 µl (final protein concentration approximately 0.19 mg/ml) intestinal microsomes in 50 mM HEPES buffer pH 7.4 (15 mM $MgCl_2$, 0.1 mM EDTA) at 37^{o}C for approximately 50 s before the reaction was started by addition of 20 µL NADPH (42 mg/ml). The total reaction volume was 1 ml. Fluorescein fluorescence was recorded using an F-4500 fluorescence spectrophotometer (Hitachi, Tokyo, Japan), excitation 485 nm and emission 538 nm. Fluorescein standard (10 µl, 25 µM) was injected into the reaction cuvette approximately 150 s after the addition of NADPH. Slopes of the linear part of time course of the product accumulation were calculated using FL-Solution 2.0 (Hitachi).

TRZ (50 µM) was incubated with liver or duodenum microsomes (0.25 mg protein/ml) and NADPH (1 mM) in 50 mM HEPES buffer (pH 7.4) supplemented with $MgCl_2$ (15 mM) and EDTA (0.1 mM) at 37°C. The reaction volume was 200 µl. After 15 min, the reaction was stopped by taking a 100 µl aliquot of the reaction mixture and adding it to an equal volume of ice-cold acetonitrile, containing dextrophan (internal standard). Samples were centrifuged for 15 minutes at approximately 3,000xg on a Legend RT centrifuge (Sorvall, Newton, CT) and the concentration of 1-hydroxytriazolam was measured by LC-MS/MS. Chromatographic separation was performed on a Phenomenex Luna, C18 column (5µm, 150 x 2 mm with Phenomenex C18 Security Guard column) (Phenomenex, Torrance, CA) using an injection volume of 10 µl and a run time of 5 minutes. The detector used was a Micromass Quattro Micro mass spectrometer (Waters) run in electrospray positive ion mode. The multiple reaction monitoring parameters for α-hydroxytriazolam were: parent ion 359 and daughter ion 176, respectively.

MDZ (10 µM) was incubated with liver and duodenum microsomes as described for TRZ. The reaction was stopped after 3 min and then further processed as described for TRZ, apart from the fact that the injection volume was 5 µl. The multiple reaction monitoring parameters were: parent ion 342 for both metabolites and daughter ion 324 and 325 for 1'-hydroxymidazolam and 4-hydroxymidazolam, respectively.

Testosterone (200 µM) was incubated with liver (final protein concentration approximately 1.5 mg/ml) or duodenum (final protein concentration 0.77 mg/ml) microsomes and NADPH (1 mM) in HEPES buffer (50 mM, pH7.4, 10 mM $MgCl_2$) for 10 min at 37^{o}C. Total reaction volume was 1 ml. The reaction was stopped by addition of methanol (300 µL) containing corticosterone as an internal standard. Samples were extracted with methylene chloride (5 ml) and the organic phase was evaporated to dryness under a stream of nitrogen. Prior to analysis samples were reconstituted in methanol and concentration of 6ß-hydroxytestosterone was determined by HPLC with UV detection. Chromatographic separation was performed on a Thermo ODS Hypersil column (5 µm, 250 x 4.6 mm) (Thermo Fisher Scientific Inc., Waltham, MA) using an injection volume of 10 µl and a run time of 50 minutes.

Supplementary TABLE 1

Determination of genotypes.

PCR primers and primer combinations used to determine the genotype of WT, $Cyp3a^{-/-}$ /$Cyp3a13^{+/+}$ and huCYP3A4/3A7 mice.

Detected allele	Primers	Expected fragment
WT mouse *Cyp3a* Cluster	5’ tcatctcctcctttcccagc 5’ gttagcctgagagccacctg	427 bp
$Cyp3a^{-/-}$/$Cyp3a13^{+/+}$	5’ gacattgacatccactttgcc 5’ gggagggaaacttggagg	319 bp
huCYP3A4/3A7	5’ cttgcccacgcctatgtcc 5’ caatggaacagaacagagccc	285 bp

Supplementary TABLE 2

qRT-PCR analysis of *CYP3A4*, *CYP3A7* and *Cyp3a13* mRNA expression in liver and duodenum of huCYP3A4/3A7 and huPXR/huCAR/huCYP3A4/3A7 mice.

huCYP3A4/3A7 (h3A4/3A7) and huPXR/huCAR/hCYP3A4/3A7 (hP/hC/h3A4/3A7) mice were treated by i.p. injection with either vehicle (VEH), RIF (10 mg/kg daily for 3 days) or PCN (10 mg/kg daily for 2 days). Data were analysed using comparative cycling time methodology, in which fluorescent output, measured as Ct, was directly proportional to input cDNA concentration. Ct values >35 were interpreted as being at the limit of detection of the TaqMan and therefore not quantitatively analyzed. The corresponding fields are left empty. ΔCt values were calculated by the subtraction of the Ct value for the internal standard β-actin of the corresponding mouse and tissue from the Ct value for each gene of interest. In all cases n=3 for huCYP3A4/3A7 and n=2 for huPXR/huCAR/huCYP3A4/3A7 mice per treatment.

			CYP3A4			CYP3A7			Cyp3a13		
	Mouse line	Treatment	Mean Ct	Mean ΔCt	St Dev ΔCt	Mean Ct	Mean ΔCt	St Dev ΔCt	Mean Ct	Mean ΔCt	St Dev ΔCt
Liver	h3A4/3A7	VEH	28.3	7.8	1.6				25.5	5.0	0.2
	hP/hC/h3A4/3A7	VEH	27.4	7.4	1.4				25.2	5.2	0.3
	h3A4/3A7	RIF	28.0	7.8	2.9				25.5	5.2	0.7
	h3A4/3A7	PCN	21.9	2.3	0.3	32.7	13.1	0.8	24.6	5.0	0.3
	hP/hC/h3A4/3A7	RIF	19.8	-0.5	0.3	30.7	10.4	0.6	24.7	4.4	0.5
	hP/hC/h3A4/3A7	PCN	26.2	6.0	0.1				24.6	4.5	0.0
Duodenum	h3A4/3A7	VEH	24.2	6.6	0.7				25.5	7.8	0.4
	hP/hC/h3A4/3A7	VEH	24.2	5.9	0.9				25.2	6.9	0.3
	h3A4/3A7	RIF	24.3	7.0	0.6				25.5	8.2	0.6
	h3A4/3A7	PCN	22.0	4.6	0.8				24.6	7.2	0.5
	hP/hC/h3A4/3A7	RIF	21.9	4.8	0.2				24.7	7.6	0.4
	hP/hC/h3A4/3A7	PCN	23.6	5.4	0.8				24.6	6.4	0.4

Supplementary Text 1

Expression of Cyp3a13 and Cyp2c55 in Cyp3a$^{-/-}$/3a13$^{+/+}$, huCYP3A4/3A7 and huPXR/huCAR/huCYP3A4/3A7 mice. As *Cyp3a13* is the only mouse *Cyp3a* gene still present in the different transgenic mouse lines, we wanted to assess whether there are compensatory changes in the expression of this gene in any of the models and if *Cyp3a13* expression is induced in the liver or intestine by PCN or RIF treatment. We therefore performed qRT-PCR analysis for *Cyp3a13* in WT, Cyp3a$^{-/-}$/3a13$^{+/+}$, huCYP3A4/3A7 and huPXR/huCAR/huCYP3A4/3A7 mice. No changes in the expression of *Cyp3a13* could be observed in any of the transgenic mouse lines and WT animals (data not shown). Furthermore, no induction of this gene was observed either in the liver or intestine of PCN or RIF treated huCYP3A4/3A7 and huPXR/huCAR/huCYP3A4/3A7 mice (Supplementary Table 2 and Supplementary Fig. 1A, B) or Cyp3a$^{-/-}$/3a13$^{+/+}$ animals (data not shown).

It has been previously reported that the expression of hepatic *Cyp2c55* mRNA is strongly induced by more than 30-fold in a *Cyp3a* knockout mouse line (van Waterschoot et al., 2008). Interestingly, hepatic *Cyp2c55* mRNA levels were only slightly increased by 4.7-fold in our Cyp3a$^{-/-}$/3a13$^{+/+}$ mice ($p<0.01$). In the huCYP3A4/3A7 and huPXR/huCAR/huCYP3A4/3A7 animals no statistically significant changes in *Cyp2c55* mRNA levels were measured relative to the WT animals (data not shown). *Cyp2c55* mRNA was, however, inducible by PCN and RIF, being increased by 7.2-fold in PCN treated huCYP3A4/3A7 mice and by 22-fold in RIF-treated huPXR/huCAR/huCYP3A4/3A7 animals (Supplementary Fig. 1C). The *Cyp2c55* induction in the Cyp3a$^{-/-}$/3a13$^{+/+}$ mice was very similar to huCYP3A4/3A7 animals (data not shown). Though the same trend of *Cyp2c55* induction was observed in the duodenum of the different mouse lines, the response was much weaker than in the liver and none of these changes were statistically significant (Supplementary Fig. 1D).